Chaos, Solitons & Fractals: X 11 (2023) 100100

Contents lists available at ScienceDirect

Chaos, Solitons & Fractals: X

journal homepage: www.elsevier.com/locate/csfx

Analysis of perturbation factors and fractional order derivatives for the novel singular model using the fractional Meyer wavelet neural networks

Zulqurnain Sabir [a,c], Mohamed R. Ali [b,d,*]

[a] Department of Mathematics and Statistics, Hazara University, Mansehra, Pakistan
[b] Faculty of Engineering and Technology, Future University in Egypt, New Cairo, 11835, Egypt
[c] Department of Computer Science and Mathematics, Lebanese American University, Beirut, Lebanon
[d] Basic Engineering Science Department, Benha Faculty of Engineering, Benha University, Banha, Egypt

ARTICLE INFO

Keywords:
Perturbed factors
Fractional order
Singular
Meyer wavelet neural network
Global approach
Analysis
Local scheme

ABSTRACT

In this study, an analysis of the perturbation factors and fractional order derivatives is performed for the novel singular model. The design of the perturbed fractional order singular model is presented by using the traditional form of the Lane-Emden along with the detail of singular points, fractional order, shape, and perturbed factors. The analysis of the perturbation factors and fractional order terms for the singular model is provided in two steps by taking three different values of the perturbed term as well as fractional order derivatives. The numerical analysis of the perturbation and fractional order terms for the novel fractional Meyer wavelet neural network (FMWNN) along with the global and local search effectiveness of the genetic algorithm (GA) and active-set algorithm (ASA) called as FMWNN-GAASA. The modeling of the FMWNN is presented in terms of mean square error, while the optimization is performed through the GAASA. The authentication, validation, excellence, and correctness of the singular model are observed by using the comparative performances of the obtained and the reference solutions. The stability of the proposed stochastic scheme is observed through the statistical performances for taking large datasets to present the analysis of the perturbation and fractional order terms.

1. Introduction

The singular kinds of differential models have become one of significant and interesting subjects for the scholar's community. The singular forms of the systems are not easy to solve, challenging, stiffer and difficult due to the singularity at the origin. The differential systems have a huge implication due to the variety of submissions in engineering and scientific areas, e.g., pattern creation, biological models, nonlinear circuits, fluidics, chemical reactor models, relativistic mechanics, population evolution, astrophysics, control theory of optimization and boundary layer studies [1–6]. The most important singular models are Emden-Fowler and Lane-Emden (LE). These two differential models have importance and a great history. The LE model is introduced by Lane and then Robert updated this model a few centuries ago by working on the spherical gas cloud associated with the classical law of thermodynamics. The general form of the LE model is a second order differential equation, which is given as [7,8]:

$$\begin{cases} \dfrac{d^2p}{dk^2} + \dfrac{\Delta}{k}\dfrac{dp}{dk} + q(p) = z(k), \quad \Delta \geq 1 \\ p(0) = a, \ \dfrac{dp(0)}{dk} = 0, \end{cases} \tag{1}$$

where Δ represents the shape factor, $q(p)$ is the function of p, $z(k)$ is the forcing function and $k = 0$ shows the singularity at the origin. It is not easy to solve these models due to the challenge of singularity and there have been only few numerical and analytical schemes have been presented to solve such models. Some mentioned schemes to solve the singular model of LE type given in Eq. (1) are Bernoulli collocation [9], Adomian decomposition [10,11], differential transform [12], Legendre wavelet [13], B-spline collocation [14], Chebyshev based neural networks [15], Jacobi-Gauss collocation [16], rational Bernoulli, Bessel, and Euler functions [17–19], the discontinuous local Galerkin [20], Lagrange and Jacobi operational matrix [21], machine learning [22] and many more [23–27]. The historical LE model given in Eq. (1) shows different forms by taking different values of $q(p)$. Some of the forms are mentioned as:

* Corresponding author.
E-mail address: mohamed.reda@fue.edu.eg (M.R. Ali).

https://doi.org/10.1016/j.csfx.2023.100100
Received 27 August 2022; Received in revised form 18 August 2023; Accepted 20 August 2023
Available online 21 August 2023

- If $q(p) = p^u$, then for $u = 0$ or 1, the model (1) is linear, otherwise nonlinear.
- If $q(p) = e^p$, then the model (1) shows the isothermal gas sphere.
- If $q(p) = \cos p,\ \cosh p,\ \sin p$ and $\sinh p$, etc., then the model (1) shows the nonlinearity.
- If $q(p) = (p^2 - C)^{\frac{3}{2}}$, then the model (1) takes the form of white-dwarf system, which is presented by Chandrasekhar [28].

The fractional order (FO) derivatives have been broadly investigated due to the numerous applications in control networks, physical models, engineering, and mathematical investigations. The use of the fractional calculus with the significant operators, like Riemann-Liouville [29], Caputo [30], Erdlyi-Kober [31], Weyl-Riesz [32] and Grnwald-Letnikov [33] has obtained a stimulating and valued subject for the researchers over the last thirty years. Recently, the FO derivatives have been used widely in many applications, some of them are pine wilt disease model with convex rate [34], anomalous heat transfer [35], the discrete form of the FO SITRs coronavirus system [36], spatiotemporal designs in the reaction form of the Belousov–Zhabotinskii models [37], three-species model [38], soil organic substance content via near-infrared and visible spectroscopy [39], SIDARTHE coronavirus pandemic differential system [40], mathematical Hepatitis B virus model [41], SITR fractal system [42], Bagley–Torvik mathematical model [43] and vaccination and Wolbachia on dengue transmission dynamics in the nonlinear model [44].

The fractional singular systems got more interesting, difficult, and challenging to solve the perturbed factor with the boundary layer performance. These stiff singular fractional perturbed kinds of models are not easy to present the solutions by using the standard and traditional numerical approaches. Consequently, it is essential to provide some consistent and dependable schemes to provide the numerical outcomes of these difficult systems [45–51]. A finite difference numerical scheme along with the exponential fitting based on the singular perturbed differential model is provided in [52–54]. There are many other investigations using the perturbed singularly diffusion-convection models of the second kind is given in [55], semi-linear performances of the diffusion-reaction equations are presented in [56] and the numerical mesh approach to get the solutions of the diffusion-reaction models is described in [57,58].

Based on the well-known operators of FO models, the significant applications of singular, perturbed, and FO models, the authors are interested to present the novel FO singular perturbed differential model. The numerical investigations of the perturbation and FO terms is performed by designing the novel fractional Meyer wavelet neural network (FMWNN) along with the global/local search effectiveness of the genetic algorithm (GA) and active-set algorithm (ASA) called as FMWNN-GAASA. The stochastic procedures based on the global/local search schemes have been exploited in diverse applications. Few of them are health care organizational decision-making systems [59], prediction of the outbreak of coronavirus [60], food-chain models [61], development of bankruptcy prediction models and their comparison [62], forecasting the thermal conductivity of a nanofluid [63], explosion theory [64,65], prediction of wind pressure coefficients on building surfaces [66], groundwater estimation from major physical hydrology components [67], detection and identification of Android malware using high-efficient [68] and strength prediction of concrete incorporating agricultural and construction wastes [69]. The novel features of the singular perturbed FO model are presented as:

- An analysis by taking small values of the perturbation factors and by fixing the values of the FO derivatives is presented to solve the designed model.
- Another analysis by using different FO derivatives values with fixed perturbation factor is provided for solving the LE model.
- The design of the singular perturbed FO model is presented by using the traditional/conventional form of the LE along with the detail of singular points, FO, shape, and perturbed factors.
- The analysis of the perturbation factors and FO terms to solve the singular LE model is provided in two different steps by taking three different values of the perturbed term as well as FO derivatives.
- The numerical investigations of the perturbation and FO terms is performed by designing the novel FMWNN along with the global/local search effectiveness of the GAASA.
- The modeling based on the FMWNN is presented using the designed perturbed FO singular model in terms of mean square error sense, while the optimization is performed through the GAASA.
- The correctness of the FMWNN-GAASA procedure is performed by using the comparative performances of the obtained and true solutions for solving the singular model.
- The constancy, convergence, and reliability of the proposed FMWNN-GAASA procedure is observed for solving the singular perturbed FO model using different statistical measures based on the semi-interquartile range (SIR), variance account for (VAF) and mean square error (MSE).
- Alongside the accurate presentations of the FMWNN-GAASA procedure, stability, robustness, comprehensive potency, smooth actions, and ease of understanding are other important features.

The rest of the paper sections are presented as: Section 2 describes the design of the singular perturbed FO model. The FMWNN-GAASA procedure is presented in Section 3. The analysis of the results is present in Section 4. The conclusions and the future research directions are presented in the last Section.

2. Design of singular perturbed FO model

The construction of the singular perturbed FO model is presented in this section using the procedural steps of the standard LE equation. In recent years, the design of various singular models has been presented, like 2nd and 3rd order pantograph models, 2nd order delay singular model, functional 4th order singular system, singular 5th and 6th kinds of differential models [60,61]. Based on these singular models, the authors are interested to solve the singular perturbed FO model. The design of the singular perturbed FO model using the standard LE model is given as [70,71]:

$$\varepsilon k^{-\Delta}\frac{d^s}{dk^s}\left(k^{\Delta}\frac{d^r}{dk^r}\right)p(k) + q(p) = z(k), \tag{2}$$

where Δ shows a real value of positive constant. For the singular perturbed FO model, the s and r values are selected as:

$$s = 1,\ r = \beta,\ \text{where } 0 < \beta < 1. \tag{3}$$

The updated form of the Eq. (2) using the Eq. (3) becomes as:

$$\varepsilon k^{-\Delta}\frac{d}{dk}\left(k^{\Delta}\frac{d^{\beta}}{dk^{\beta}}\right)p(k) + q(p) = z(k), \tag{4}$$

the simplified form of one of the factors in Eq. (4) is given as:

$$\frac{d}{dk}\left(k^{\Delta}\frac{d^{\beta}}{dk^{\beta}}\right)p(k) = k^{\Delta}\frac{d^{\beta+1}}{dk^{\beta+1}}p(k) + \Delta k^{\Delta-1}\frac{d^{\beta}}{dk^{\beta}}p(k). \tag{5}$$

The obtained mathematical formulation is given as:

$$\begin{cases} \varepsilon \dfrac{d^{\beta+1}}{dk^{\beta+1}} p(k) + \varepsilon \dfrac{\Delta}{k} \dfrac{d^{\beta}}{dk^{\beta}} p(k) + q(p) = z(k), \\ p(0) = 0, \ \ p(1) = 0. \end{cases} \tag{6}$$

The above form of the mathematical model is known as singular perturbed FO model, where the single singularity and shape factor arises at k and Δ, respectively. While the perturbed factors arise twice in 1st and 2nd factor. Fig. 1 shows the flowchart illustrations of the singular perturbed FO model.

3. Methodology

In this section, the design of the FMWNN-GAASA procedure is presented using the Meyer wavelet neural networks. The construction of the differential systems, merit function and the optimization procedure using the hybrid GAASA is also described.

3.1. Merit function: FMWNN procedure

The designed methodology based on the FMWNN procedure is provided in this section, $\widehat{p}(k)$ indicates the proposed solutions the proposed system, $\frac{d^{(n)}}{dk^{(n)}}\widehat{p}(k)$and $\frac{d^{\beta}}{dk^{\beta}}\widehat{p}(k)$ represent the n^{th} integer and fractional form of the derivatives, respectively. The system networks are presented as:

$$\begin{aligned} \widehat{p}(k) &= \sum_{i=1}^{m} m_i A(w_i k + j_i) \\ \frac{d^{(n)}}{dk^{(n)}} \widehat{p}(k) &= \sum_{i=1}^{m} m_i \frac{d^{(n)}}{dk^{(n)}} A(w_i k + j_i), \\ \frac{d^{\beta}}{dk^{\beta}} \widehat{p}(k) &= \sum_{i=1}^{m} m_i \frac{d^{\beta}}{dk^{\beta}} A(w_i k + j_i) \end{aligned} \tag{7}$$

where, m presents the neurons, $\boldsymbol{m}$, $\boldsymbol{w}$ and $\boldsymbol{j}$ are the vector mechanisms of the weights $\boldsymbol{W}$, given as:

$$\boldsymbol{W} = [\boldsymbol{m}, \boldsymbol{w}, \boldsymbol{j}], \ \text{for } \boldsymbol{m} = [m_1, m_2, ..., m_m], \ \boldsymbol{w} = [w_1, w_2, ..., w_m] \ \textit{and } \boldsymbol{j} = [j_1, j_2, ..., j_m].$$

The Meyer wavelet merit function is presented as:

$$A(k) = 35k^4 - 84k^5 + 70k^6 - 20k^7. \tag{8}$$

The restructured form of Eq. (7) with the use of Eq. (8) is shown as:

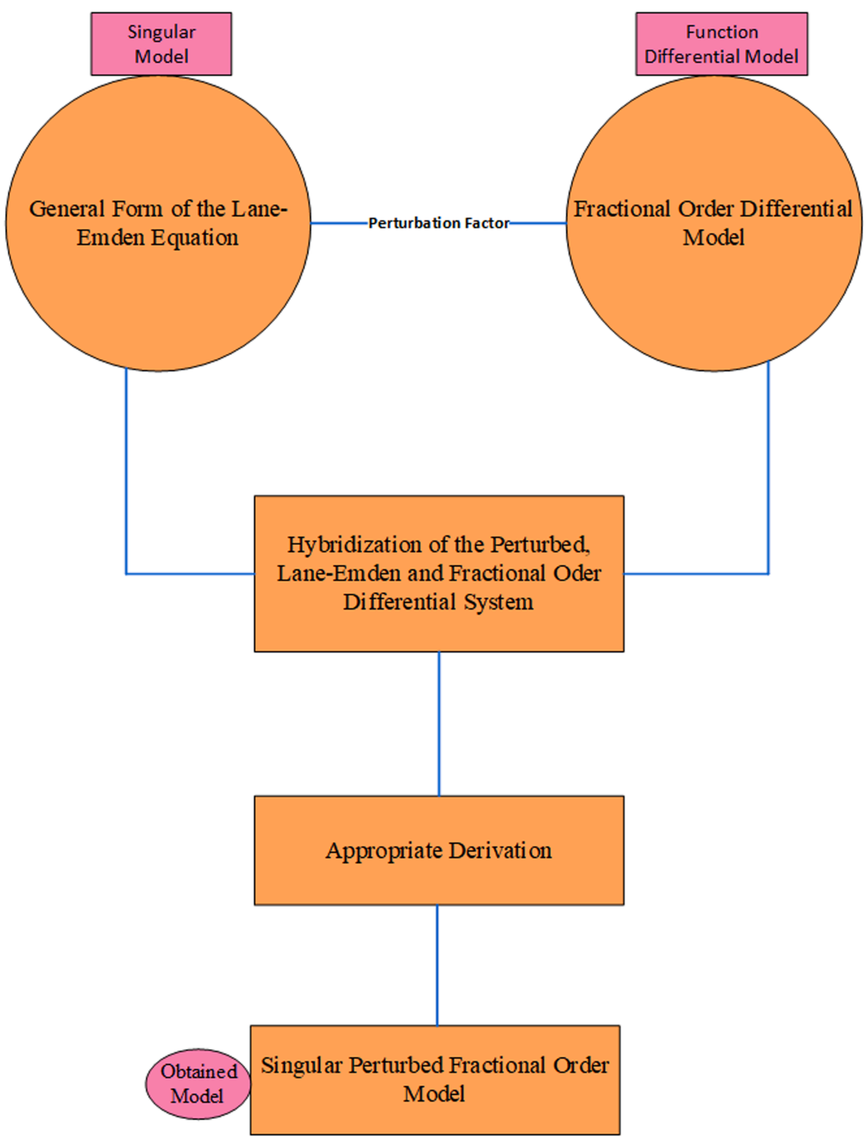

Fig 1. Flow-chart illustrations of the singular perturbed FO model.

$$\begin{aligned}
&\widehat{p}(k)=\sum_{i=1}^{m} m_i\left(35(w_ik+j_i)^4-84(w_ik+j_i)^5+70(w_ik+j_i)^6-20(w_ik+j_i)^7\right),\\
&\frac{d^{(n)}}{dk^{(n)}}\widehat{p}(k)=\sum_{i=1}^{m} m_i\begin{pmatrix}35\frac{d^{(n)}}{dk^{(n)}}A(w_ik+j_i)^4-84\frac{d^{(n)}}{dk^{(n)}}A(w_ik+j_i)^5+70\frac{d^{(n)}}{dk^{(n)}}A(w_ik+j_i)^6\\-20\frac{d^{(n)}}{dk^{(n)}}A(w_ik+j_i)^7\end{pmatrix},\\
&\frac{d^{\beta}}{dk^{\beta}}\widehat{p}(k)=\sum_{i=1}^{m} a_i\begin{pmatrix}35\frac{d^{\beta}}{dk^{\beta}}A(w_ik+j_i)^4-84\frac{d^{\beta}}{dk^{\beta}}A(w_ik+j_i)^5+70\frac{d^{\beta}}{dk^{\beta}}A(w_ik+j_i)^6\\-20\frac{d^{\beta}}{dk^{\beta}}A(w_ik+j_i)^7\end{pmatrix}.
\end{aligned} \tag{9}$$

For the estimated ANN weights, a merit function E_M is shown as:

$$E_M=E_{M-1}+E_{M-2}. \tag{10}$$

Where, $E_{M-1}$and E_{M-2} present the merit functions based on the singular perturbed FO model shown in Eq. (6) is given as:

$$E_{M-1}=\frac{1}{N}\sum_{i=1}^{m}\left(\varepsilon\frac{d^{\beta+1}}{dk^{\beta+1}}\widehat{p}_m+\varepsilon\frac{\Delta}{k_m}\frac{d^{\beta}}{dk^{\beta}}\widehat{p}_m+q(\widehat{p}_m)-z_m\right)^2, \tag{11}$$

$$E_{M-2}=\frac{1}{2}\left((\widehat{p}_0)^2+(\widehat{p}_N)^2\right), \tag{12}$$

here $\widehat{p}_m=\widehat{p}(k_m),\ z_m=z(k_m)\ Nh=1$ and $k_m=mh$. The solution of the singular perturbed FO model given in the Eq. (6) is provided with the accessibility of suitable weights $\boldsymbol{W}$, i.e., $E_M\rightarrow 0$, the proposed MWNN solutions become alike with the optimal solutions, i.e., $[\widehat{p}\rightarrow p]$.

3.2. Optimization of the networks

The optimization of the networks based on the FMNN is provided by applying the hybridization procedures of the GAASA for the numerical solutions of the singular perturbed FO model.

The global search GA provides an efficient constrained or unconstrained optimization search approach, which is expressed in the form of mathematical processes of genetic natural performance. In the process of GA, the individual population frequently alters, i.e., candidate optimization project solution and the capability to perform the abundant optimization models by merging its imitation apparatuses via selection measures, crossover process, mutation procedure, and elitism framework. Some updated applications proposed by the GA are the identification of the parameter using the multivariable models [72], best weight constructions based on the steel space borders [73], controlling of the car's robot [74], thickness of the layer optimization of piezoelectric multilayer transducer [75], parameters approximation based on the electromagnetic waves of plane [76] and combined load dispatch models connecting both wind and thermal generators [77]. The slowness and indolence of GA is reduced through the hybridization performances with the local algorithms along with the improved optimization process.

ASA is known as an efficient and quick local search approach based on the modification of optimization in various proposals arising in the multiplicity. ASA represents a systematized convex optimization scheme that is oppressed for constrained and unconstrained modeling. Recently, the ASA is used in non-negative matrix factorization [78], pressure-dependent models of water distribution systems with flow controls [79], linearly constrained non-Lipschitz nonconvex optimization [80], a quasi-monolithic phase-field description for orthotropic anisotropic fracture [81], embedded model predictive control [82] and large-scale non-smooth optimization models with box constraints [83].

3.3. Statistical performance

The proposed investigations represent the three different forms of the statistical performances based on the VAF, SIR, and MSE. The mathematical formulations of the exact results p and proposed outcomes $\widehat{p}$ are shown as:

$$\text{VAF}=\left(1-\frac{\text{var}(p_i-\widehat{p}_i)}{\text{var}(p_i)}\right)\times 100, \tag{13}$$

$$\text{MSE}=\sum_{i=1}^{k}(p_i-\widehat{p}_i)^2, \tag{14}$$

$$\text{SIR}=\frac{1}{2}\left(3^{\text{rd}}\text{ Quartile}-1^{\text{st}}\text{Quartile}\right). \tag{15}$$

Fig. 2 shows the proposed hybridization procedures based on the GAASA for the numerical solutions of the singular perturbed FO model. In this figure, the designed singular perturbed FO model, proposed modeling based on the ANNs structure, proposed methodology based on the GAASA, storage of the data and results performance structure is provided.

4. Simulations and results

The current section performs the detailed numerical simulations for the numerical solutions of the singular perturbed FO model. The single, output/input and the hidden layers based on the MWNN is provided in the modeling of Eq. (6) using the system (10 to 12), while the optimization toolbox that is inbuilt Matlab solver is to train the weight vectors of the MWNN models to solve the singular perturbed FO model. The proposed results based on the FMWNN-GAASA are designed on the basis of multiple runs to present the analysis of the perturbation factors and FO derivatives in the form of the graphical depictions, accuracy and convergence. The mathematical formulations of the singular perturbed FO model shown in Eq. (6) is multiplied by k becomes as:

$$\begin{cases}\varepsilon k\frac{d^{\beta+1}}{dk^{\beta+1}}p(k)+\Delta\varepsilon\frac{d^{\beta}}{dk^{\beta}}p(k)+kq(p)=kz(k)=L(k),\\ p(0)=0,\ \ p(1)=0.\end{cases} \tag{16}$$

where,

$$L(k)=\varepsilon k\left(\frac{\Gamma(m+1)}{\Gamma(m-\beta)}k^{m-\beta-1}-\frac{\Gamma(n+1)}{\Gamma(n-\beta)}k^{n-\beta-1}\right)+\Delta\varepsilon\left(\frac{\Gamma(m+1)}{\Gamma(m-\beta+1)}k^{m-\beta}-\frac{\Gamma(n+1)}{\Gamma(n-\beta+1)}k^{n-\beta}\right)+k^{m+2}-k^{n+2}, \tag{17}$$

where m and n are taken as positive. The update form using the Eqs. (16) and (17) is given as:

$$\begin{cases}\varepsilon k\frac{d^{\beta+1}}{dk^{\beta+1}}p(k)+\Delta\varepsilon\frac{d^{\beta}}{dk^{\beta}}p(k)+kq(p)=\varepsilon k\left(\frac{\Gamma(m+1)}{\Gamma(m-\beta)}k^{m-\beta-1}-\frac{\Gamma(n+1)}{\Gamma(n-\beta)}k^{n-\beta-1}\right)\\ +\Delta\varepsilon\left(\frac{\Gamma(m+1)}{\Gamma(m-\beta+1)}k^{m-\beta}-\frac{\Gamma(n+1)}{\Gamma(n-\beta+1)}k^{n-\beta}\right)+k^{m+2}-k^{n+2},\\ p(0)=0,\ p(1)=0.\end{cases} \tag{18}$$

The exact solution of the singular perturbed FO model (18) is shown as:

$$p(k)=k^m-k^n. \tag{19}$$

The updated form of Eq. (19) by taking the values of $m=2$ and $n=1$ is given as:

$$p(k)=k^2-k. \tag{20}$$

4.1. Analysis of perturbation factor

In this section, three different perturbation cases by taking small values are provided by using fixed values the FO derivatives.

Case 1: Consider the singular perturbed FO model (18) with $\beta=0.1$, $\Delta=2$ and $\varepsilon=\frac{1}{2^2}$ is given as:

$$\begin{cases}\frac{1}{4}k\frac{d^{1.1}}{dk^{1.1}}p(k)+\frac{1}{2}\frac{d^{0.1}}{dk^{0.1}}p(k)+kq(p)=\frac{1}{4}\left(\frac{2}{\Gamma(1.9)}+\frac{4}{\Gamma(2.9)}\right)k^{1.9}-\frac{1}{4}\left(\frac{1}{\Gamma(0.9)}+\frac{2}{\Gamma(1.9)}\right)k^{0.9}+k^3-k^2,\\ p(0)=0,\quad p(1)=0.\end{cases} \tag{21}$$

A merit function for the Eq. (21) is given as:

$$E_M=\frac{1}{N}\sum_{i=1}^{m}\left(\frac{1}{4}k_m\frac{d^{1.1}}{dk^{1.1}}\widehat{p}_m+\frac{1}{2}\frac{d^{0.1}}{dk^{0.1}}\widehat{p}_m+k_mq_m-\frac{1}{4}\left(\frac{2}{\Gamma(1.9)}+\frac{4}{\Gamma(2.9)}\right)k_m^{1.9}+\frac{1}{4}\left(\frac{1}{\Gamma(0.9)}+\frac{2}{\Gamma(1.9)}\right)k_m^{0.9}-k_m^3+k_m^2\right)^2+\frac{1}{2}\left((\widehat{p}_0)^2+(\widehat{p}_m)^2\right) \tag{22}$$

Case 2: Consider the singular perturbed FO model (18) with $\beta=0.1$, $\Delta=2$ and $\varepsilon=\frac{1}{2^3}$ is given as:

$$\begin{cases}\frac{1}{8}k\frac{d^{1.1}}{dk^{1.1}}p(k)+\frac{1}{4}\frac{d^{0.1}}{dk^{0.1}}p(k)+kq(p)=\frac{1}{8}\left(\frac{2}{\Gamma(1.9)}+\frac{4}{\Gamma(2.9)}\right)k^{1.9}-\frac{1}{8}\left(\frac{1}{\Gamma(0.9)}+\frac{2}{\Gamma(1.9)}\right)k^{0.9}+k^3-k^2,\\ p(0)=0,\quad p(1)=0.\end{cases} \tag{23}$$

A merit function for the Eq. (23) is given as:

$$E_M=\frac{1}{N}\sum_{i=1}^{m}\left(\frac{1}{8}k_m\frac{d^{1.1}}{dk^{1.1}}\widehat{p}_m+\frac{1}{4}\frac{d^{0.1}}{dk^{0.1}}\widehat{p}_m+k_mq_m-\frac{1}{8}\left(\frac{2}{\Gamma(1.9)}+\frac{4}{\Gamma(2.9)}\right)k_m^{1.9}+\frac{1}{8}\left(\frac{1}{\Gamma(0.9)}+\frac{2}{\Gamma(1.9)}\right)k_m^{0.9}-k_m^3+k_m^2\right)^2+\frac{1}{2}\left((\widehat{p}_0)^2+(\widehat{p}_m)^2\right) \tag{24}$$

Case 3: Consider the singular perturbed FO model (18) with $\beta=0.1$, $\Delta=2$ and $\varepsilon=\frac{1}{2^4}$ is given as:

$$\begin{cases}\frac{1}{16}k\frac{d^{1.1}}{dk^{1.1}}p(k)+\frac{1}{8}\frac{d^{0.1}}{dk^{0.1}}p(k)+kq(p)=\frac{1}{16}\left(\frac{2}{\Gamma(1.9)}+\frac{4}{\Gamma(2.9)}\right)k^{1.9}-\frac{1}{16}\left(\frac{1}{\Gamma(0.9)}+\frac{2}{\Gamma(1.9)}\right)k^{0.9}+k^3-k^2,\\ p(0)=0,\quad p(1)=0.\end{cases} \tag{25}$$

A merit function for the Eq. (25) is given as:

$$E_M = \frac{1}{N}\sum_{i=1}^{m}\left(\begin{array}{l}\frac{1}{16}k_m\frac{d^{1.1}}{dk^{1.1}}\widehat{p}_m + \frac{1}{8}\frac{d^{0.1}}{dk^{0.1}}\widehat{p}_m + k_m q_m - \frac{1}{16}\left(\frac{2}{\Gamma(1.9)}+\frac{4}{\Gamma(2.9)}\right)k_m^{1.9}\\ +\frac{1}{16}\left(\frac{1}{\Gamma(0.9)}+\frac{2}{\Gamma(1.9)}\right)k_m^{0.9} - k_m^3 + k_m^2\end{array}\right)^2 + \frac{1}{2}\left((\widehat{p}_0)^2 + (\widehat{p}_m)^2\right) \tag{26}$$

The performance of each case of the singular perturbed FO model is provided by using the optimization procedures based on the GAASA. The stochastic iterative procedure replicates forty executions to perform a greater dataset based on the parameters of the MWNN. The accomplished MWNN weight vectors are provided in the first set of Eq. (9) to evaluate the proposed outcomes for each variation of the singular perturbed FO model. The formulations are provided for case 1 to 3 of the singular perturbed FO model are presented as:

$$\begin{aligned}\widehat{p}_{case-1} = & -0.016\left(35(1.528k-0.4368)^4 - 84(1.528k-0.4368)^5 + 70(1.528k-0.4368)^6 - 20(1.528k-0.4368)^7\right)\\ & +0.9229\left(35(-0.26k+0.1409)^4 - 84(-0.26k+0.1409)^5 + 70(-0.26k+0.1409)^6 - 20(-0.26k+0.140)^7\right)\\ & -0.3689\left(35(1.333k-0.1116)^4 - 84(1.333k-0.1116)^5 + 70(1.333k-0.1116)^6 - 20(1.333k-0.1116)^7\right)\\ & +\ldots+3.0335\left(35(0.007k+0.0345)^4 - 84(0.007k+0.0345)^5 + 70(0.007k+0.0345)^6 - 20(0.007k+0.0345)^7\right),\end{aligned} \tag{27}$$

$$\begin{aligned}\widehat{p}_{case-2} = & -0.171\left(35(0.048k+1.1747)^4 - 84(0.048k+1.1747)^5 + 70(0.048k+1.1747)^6 - 20(0.048k+1.1747)^7\right)\\ & -0.0231\left(35(0.426k+0.8044)^4 - 84(0.426k+0.8044)^5 + 70(0.426k+0.8044)^6 - 20(0.426k+0.8044)^7\right)\\ & +1.6154\left(35(-0.327k+0.478)^4 - 84(-0.327k+0.478)^5 + 70(-0.327k+0.478)^6 - 20(-0.32k+0.478)^7\right)\\ & +\ldots+1.1114\left(35(-0.168k+1.0768)^4 - 84(-0.168k+1.07)^5 + 70(-0.168k+1.076)^6 - 20(-0.168k+1.076)^7\right),\end{aligned} \tag{28}$$

$$\begin{aligned}\widehat{p}_{case-3} = & \ 0.697\left(35(0.024k+1.2501)^4 - 84(0.024k+1.2501)^5 + 70(0.0240k+1.2501)^6 - 20(0.0240k+1.2501)^7\right)\\ & -1.081\left(35(-0.65k+1.5890)^4 - 84(-0.65k+1.5890)^5 + 70(-0.650k+1.5890)^6 - 20(-0.650k+1.589)^7\right)\\ & -0.448\left(35(0.857k-0.0969)^4 - 84(0.857k-0.0969)^5 + 70(0.857k-0.0969)^6 - 20(0.857k-0.0969)^7\right)\\ & +\ldots+1.3111\left(35(0.169k+0.6908)^4 - 84(0.169k+0.6908)^5 + 70(0.169k+0.6908)^6 - 20(0.169k+0.6908)^7\right),\end{aligned} \tag{29}$$

The proposed results are performed in Eqs. (27)–(29) along with the graphically representations of these results are performed in Fig. 3(a–c), while the mean, best and worst results comparison is provided in Fig. 3 (d–f) for the perturbed cases 1 to 3. The overlapping of the mean, best and worst results is performed for each perturbed case, which represent the exactness of the FMWNN-GAASA approach. The absolute error (AE) performances are presented in Fig. 3(g) for the perturbed case of the singular model. The best AE performances are reported as 10^{-08} to 10^{-10}, 10^{-07} to 10^{-08} and 10^{-06} to 10^{-07} for 1st, 2nd and 3rd case. It is observed that the perturbation factor is performed good for case 1 as compared to other two cases. Fig. 4 shows the performance measures for the perturbed case 1 to 3 to solve the singular differential model. The scale of the performance gages using the Fitness (Fit), VAF and MSE operators for each perturbed case is given in Fig. 4. The Fit performances calculated closed to 10^{-16} for perturbed case 1, while for perturbed cases 2 and 3, the Fit measures lie between 10^{-15} and 10^{-16}, respectively. The EVAF measures are calculated for perturbed case 1 closed to 10^{-15}, 10^{-13} and 10^{-14} for perturbed cases 2 and the EVAF measures found in between 10^{-12} and 10^{-13} for case 3 of the singular differential model. The MSE measures for perturbed case 1 are performed in between 10^{-12} to 10^{-13} and 10^{-11} to 10^{-12} for perturbed cases 1 and 2, while for perturbed case 3, these values performed around 10^{-11} to solve the singular differential model. It is also performed through the performance indices that the case 1 performs very well as compared to other two perturbed based cases.

The convergence plots based on the statistical Fit, VAF and MSE together with histograms (HGs) and boxplots (BPs) are derived in Figs. 5 to 6. The Fit measures are derived in Fig. 5 for each perturbed case of the singular model. The Fit values are calculated as 10^{-08} to 10^{-13}, 10^{-08} to 10^{-10}, 10^{-06} to 10^{-09} for each perturbed case of the singular model. The EVAF measures are reported in Fig. 6, which is around 10^{-07} to 10^{-15}, 10^{-05} to 10^{-10}, 10^{-04} to 10^{-08} for each perturbed case of the singular model. It is concluded on the behalf of these results that more than 80% executions achieved reasonable and precise level of the statistical results. It is observed that the performances of the case 1 are better as compared to other two perturbed cases of the singular differential model.

The analysis of the perturbation factor is further analyzed in Table 1 by taking minimum, maximum, standard deviation (STD), mean, SIR and median operators for 40 executions for solving the singular models. The minimum values represent the best performances, while the opposite behavior is noticed in the case of maximum operators. The minimum values for the perturbation factor cases are provided as 10^{-09} to 10^{-10}, 10^{-08} to 10^{-09} and 10^{-07} to 10^{-08}. The maximum gages are performed even bad result and found as 10^{-02} to 10^{-03} for each perturbation case of the singular model. The mean measures for the perturbation factor cases are performed as 10^{-04} to 10^{-05}, 10^{-03} to 10^{-05} and 10^{-02} to 10^{-04}. The median representations for the perturbation factor case 1–3 are reported as 10^{-05} to 10^{-06}, 10^{-04} to 10^{-05} and 10^{-03} to 10^{-05}. The STD measures for the perturbation factor each case of the model are reported as 10^{-03} to 10^{-04}. Similarly, the SIR performances are reported in good measures for each perturbed case of the singular model.

The analysis of the perturbed singular performances of three cases is presented and it is observed that the values of the $\varepsilon = \frac{1}{2^2}$ is performed betters as compared to the values of the $\varepsilon = \frac{1}{2^3}$ and $\varepsilon = \frac{1}{2^4}$. Few witnessed points that present the performance of case 1 is better as compared to case 2 and case 3 are presented as:

- The AE performances are reported as 10^{-08} to 10^{-10}, 10^{-07} to 10^{-08} and 10^{-06} to 10^{-07} for 1st, 2nd and 3rd case.

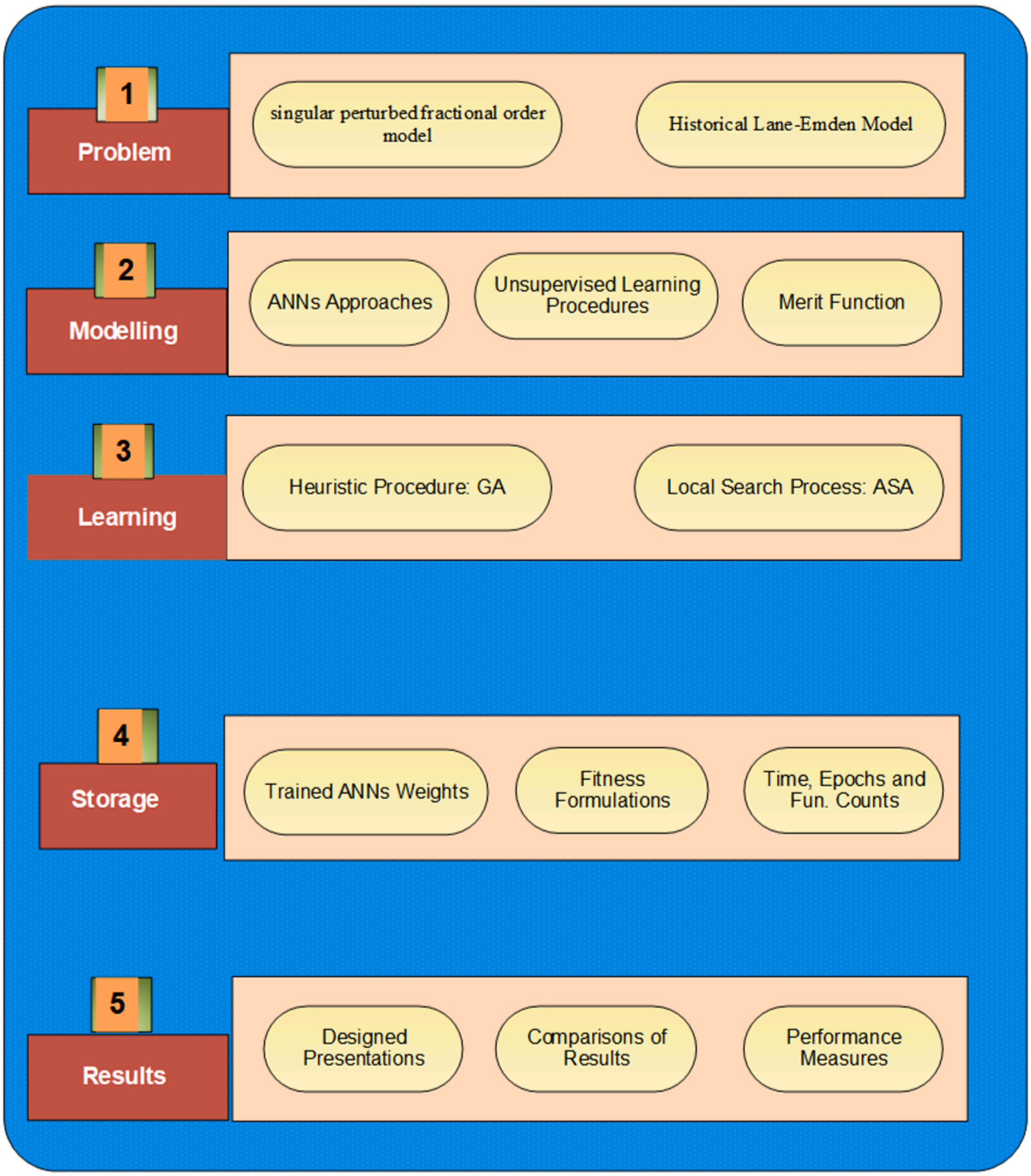

Fig. 2. FMWNN-GAASA procedure for the numerical solutions of the singular perturbed FO model.

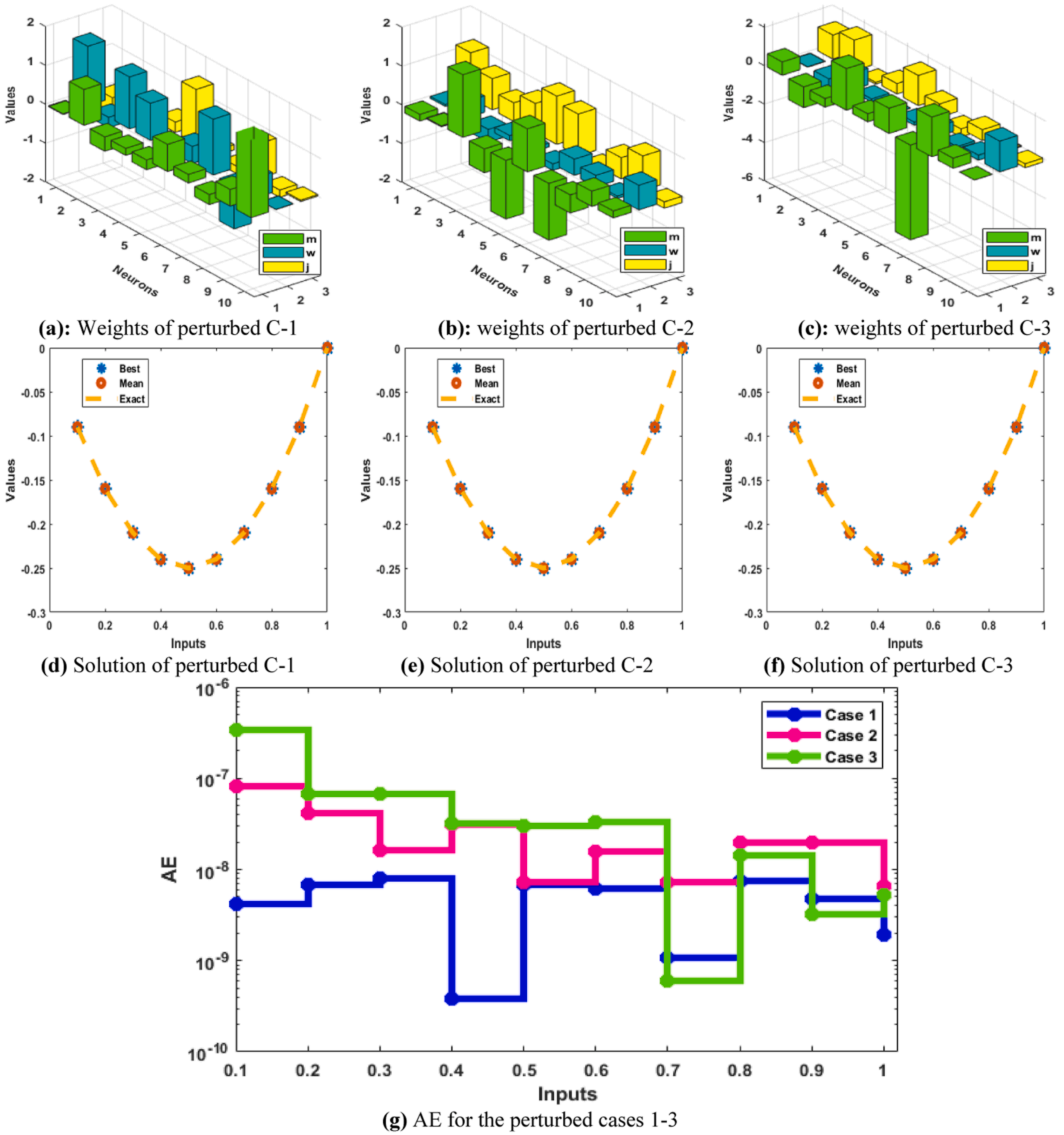

Fig. 3. Weights (a–c), solutions performances (d–f) and AE (g) for the perturbed case 1 to 3 for solving the singular differential model.

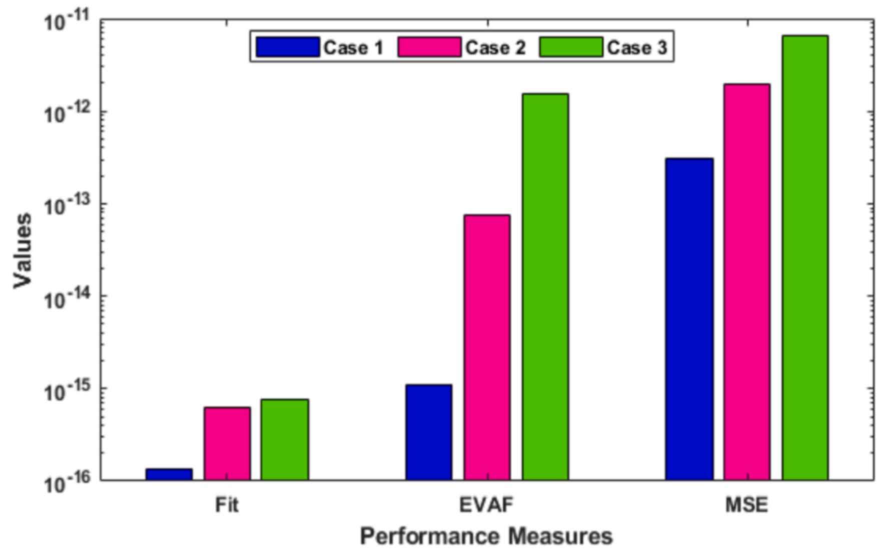

Fig. 4. Performance measures for the perturbed case 1 to 3 to solve the singular LE model.

- The performance measures for the Fit operator are performed closed to 10^{-16} for perturbed case 1, while for perturbed cases 2 and 3, the Fit measures lie between 10^{-15} and 10^{-16}, respectively.
- The EVAF measures are performed for perturbed case 1 closed to 10^{-15}, 10^{-13} and 10^{-14} for perturbed cases 2 and the EVAF measures found in between 10^{-12} and 10^{-13} for case 3 to solve the singular differential model.
- The MSE measures for perturbed case 1 are performed in between 10^{-12} to 10^{-13} and 10^{-11} to 10^{-12} for perturbed cases 1 and 2, while for perturbed case 3, these measures are reported as 10^{-11} to solve the singular differential model.
- The convergence based on the Fitness is calculated as 10^{-07} to 10^{-13}, 10^{-08} to 10^{-10}, 10^{-06} to 10^{-09} for respective perturbed cases of the singular model.
- The EVAF are reported as 10^{-07} to 10^{-15}, 10^{-05} to 10^{-10}, 10^{-04} to 10^{-08} for each perturbed case of the singular model.
- The minimum operator values for the respective perturbation factor cases are provided as 10^{-09} to 10^{-10}, 10^{-08} to 10^{-09} and 10^{-07} to 10^{-08}.
- The mean measures for the perturbation factor cases are performed as 10^{-04} to 10^{-05}, 10^{-3} to 10^{-05} and 10^{-02} to 10^{-04}.
- The median representations for the perturbation factor case 1–3 are reported as 10^{-05} to 10^{-06}, 10^{-04} to 10^{-05} and 10^{-03} to 10^{-05}.

4.2. Analysis of FO derivatives

In this section, three different cases of the FO derivatives are provided by using the fix values the perturbation factor

Case 1: Consider the singular perturbed FO model (18) with $\beta = 0.1$, $\Delta = 2$ and $\varepsilon = \frac{1}{2^5}$ is given as:

$$\begin{cases} \frac{1}{32}k\frac{d^{1.1}}{dk^{1.1}}p(k) + \frac{1}{16}\frac{d^{0.1}}{dk^{0.1}}p(k) + kq(p) = \frac{1}{32}\left(\frac{2}{\Gamma(1.9)} + \frac{4}{\Gamma(2.9)}\right)k^{1.9} - \frac{1}{32}\left(\frac{1}{\Gamma(0.9)} + \frac{2}{\Gamma(1.9)}\right)k^{0.9} + k^3 - k^2, \\ p(0) = 0, \ \ p(1) = 0. \end{cases} \tag{30}$$

A merit function for the Eq. (30) is given as:

$$E_M = \frac{1}{N}\sum_{i=1}^{m}\begin{pmatrix} \frac{1}{32}k_m\frac{d^{1.1}}{dk^{1.1}}\widehat{p}_m + \frac{1}{16}\frac{d^{0.1}}{dk^{0.1}}\widehat{p}_m + k_m q_m - \frac{1}{32}\left(\frac{2}{\Gamma(1.9)} + \frac{4}{\Gamma(2.9)}\right)k_m^{1.9} \\ +\frac{1}{32}\left(\frac{1}{\Gamma(0.9)} + \frac{2}{\Gamma(1.9)}\right)k_m^{0.9} - k_m^3 + k_m^2 \end{pmatrix}^2 + \frac{1}{2}\left((\widehat{p}_0)^2 + (\widehat{p}_m)^2\right) \tag{31}$$

Case 2: Consider the singular perturbed FO model (18) with $\beta = 0.2$, $\Delta = 2$ and $\varepsilon = \frac{1}{2^5}$ is given as:

$$\begin{cases} \frac{1}{32}k\frac{d^{1.2}}{dk^{1.2}}p(k) + \frac{1}{16}\frac{d^{0.2}}{dk^{0.2}}p(k) + kq(p) = \frac{1}{32}\left(\frac{2}{\Gamma(1.8)} + \frac{4}{\Gamma(2.8)}\right)k^{1.8} - \frac{1}{32}\left(\frac{1}{\Gamma(0.8)} + \frac{2}{\Gamma(1.8)}\right)k^{0.8} + k^3 - k^2, \\ p(0) = 0, \ \ p(1) = 0. \end{cases} \tag{32}$$

A merit function for the Eq. (32) is given as:

$$E_M = \frac{1}{N}\sum_{i=1}^{m}\left(\begin{array}{l}\frac{1}{32}k_m\frac{d^{1.2}}{dk^{1.2}}\widehat{p}_m + \frac{1}{16}\frac{d^{0.2}}{dk^{0.2}}\widehat{p}_m + k_m q_m - \frac{1}{32}\left(\frac{2}{\Gamma(1.8)}+\frac{4}{\Gamma(2.8)}\right)k_m^{1.8}\\ +\frac{1}{32}\left(\frac{1}{\Gamma(0.8)}+\frac{2}{\Gamma(1.8)}\right)k_m^{0.8} - k_m^3 + k_m^2\end{array}\right)^2 + \frac{1}{2}\left((\widehat{p}_0)^2 + (\widehat{p}_m)^2\right) \tag{33}$$

Case 3: Consider the singular perturbed FO model (18) with $\beta = 0.3$, $\Delta = 2$ and $\varepsilon = \frac{1}{2^5}$ is given as:

$$\begin{cases}\frac{1}{32}k\frac{d^{1.3}}{dk^{1.3}}p(k) + \frac{1}{16}\frac{d^{0.3}}{dk^{0.3}}p(k) + kq(p) = \frac{1}{32}\left(\frac{2}{\Gamma(1.7)}+\frac{4}{\Gamma(2.7)}\right)k^{1.7} - \frac{1}{32}\left(\frac{1}{\Gamma(0.7)}+\frac{2}{\Gamma(1.7)}\right)k^{0.7} + k^3 - k^2,\\ p(0) = 0,\ \ p(1) = 0.\end{cases} \tag{34}$$

A merit function for the Eq. (34) is given as:

$$E_M = \frac{1}{N}\sum_{i=1}^{m}\left(\begin{array}{l}\frac{1}{32}k_m\frac{d^{1.3}}{dk^{1.3}}\widehat{p}_m + \frac{1}{16}\frac{d^{0.3}}{dk^{0.3}}\widehat{p}_m + k_m q_m - \frac{1}{32}\left(\frac{2}{\Gamma(1.7)}+\frac{4}{\Gamma(2.7)}\right)k_m^{1.7}\\ +\frac{1}{32}\left(\frac{1}{\Gamma(0.7)}+\frac{2}{\Gamma(1.7)}\right)k_m^{0.7} - k_m^3 + k_m^2\end{array}\right)^2 + \frac{1}{2}\left((\widehat{p}_0)^2 + (\widehat{p}_m)^2\right) \tag{35}$$

The mathematical representations of each FO case of the singular perturbed FO model are obtained through the optimization of the GAASA procedure. The computing iterative scheme replicates for forty runs to get a larger dataset using the MWNN parameters. The proficient weights through the MWNN are given to assess the obtained results for each FO case of the singular perturbed FO model, mathematically shown as:

$$\begin{aligned}\widehat{p}_{case-1} = & -0.184\left(35(-0.219k+0.039)^4 - 84(-0.219k+0.039)^5 + 70(-0.219k+0.039)^6 - 20(-0.219k+0.039)^7\right)\\ & -0.2969\left(35(1.3214k-0.0135)^4 - 84(1.3214k-0.013)^5 + 70(1.3214k-0.0135)^6 - 20(1.3214k-0.013)^7\right)\\ & +1.2369\left(35(-0.865k+0.5574)^4 - 84(-0.865k+0.557)^5 + 70(-0.865k+0.557)^6 - 20(-0.865k+0.557)^7\right)\\ & +\ldots+00006\left(35(1.3485k-0.4082)^4 - 84(1.3485k-0.4082)^5 + 70(1.3485k-0.4082)^6 - 20(1.3485k-0.408)^7\right),\end{aligned} \tag{36}$$

$$\begin{aligned}\widehat{p}_{case-2} = & \ 0.4193\left(35(0.3232k+0.3566)^4 - 84(0.3232k+0.3566)^5 + 70(0.3232k+0.356)^6 - 20(0.3232k+0.356)^7\right)\\ & +0.0959\left(35(-1.224k+0.3166)^4 - 84(-1.224k+0.3166)^5 + 70(-1.224k+0.316)^6 - 20(-1.224k+0.316)^7\right)\\ & +1.4671\left(35(0.4170k+0.0952)^4 - 84(0.4170k+0.0952)^5 + 70(0.4170k+0.0952)^6 - 20(0.4170k+0.095)^7\right)\\ & +\ldots-1.3358\left(35(-0.566k+0.1550)^4 - 84(-0.566k+0.155)^5 + 70(-0.566k+0.1550)^6 - 20(-0.566k+0.155)^7\right),\end{aligned} \tag{37}$$

$$\begin{aligned}\widehat{p}_{case-3} = & -0.240\left(35(-0.410k+0.3551)^4 - 84(-0.410k+0.3551)^5 + 70(-0.410k+0.355)^6 - 20(-0.410k+0.355)^7\right)\\ & +1.0695\left(35(0.5146k-0.1879)^4 - 84(0.5146k-0.1879)^5 + 70(0.5146k-0.187)^6 - 20(0.5146k-0.187)^7\right)\\ & -1.0906\left(35(0.067k+0.0423)^4 - 84(0.0671k+0.0423)^5 + 70(0.0671k+0.0423)^6 - 20(0.0671k+0.0423)^7\right)\\ & +\ldots-1.7145\left(35(0.293k+0.0404)^4 - 84(0.2932k+0.0404)^5 + 70(0.2932k+0.0404)^6 - 20(0.293k+0.0404)^7\right),\end{aligned} \tag{38}$$

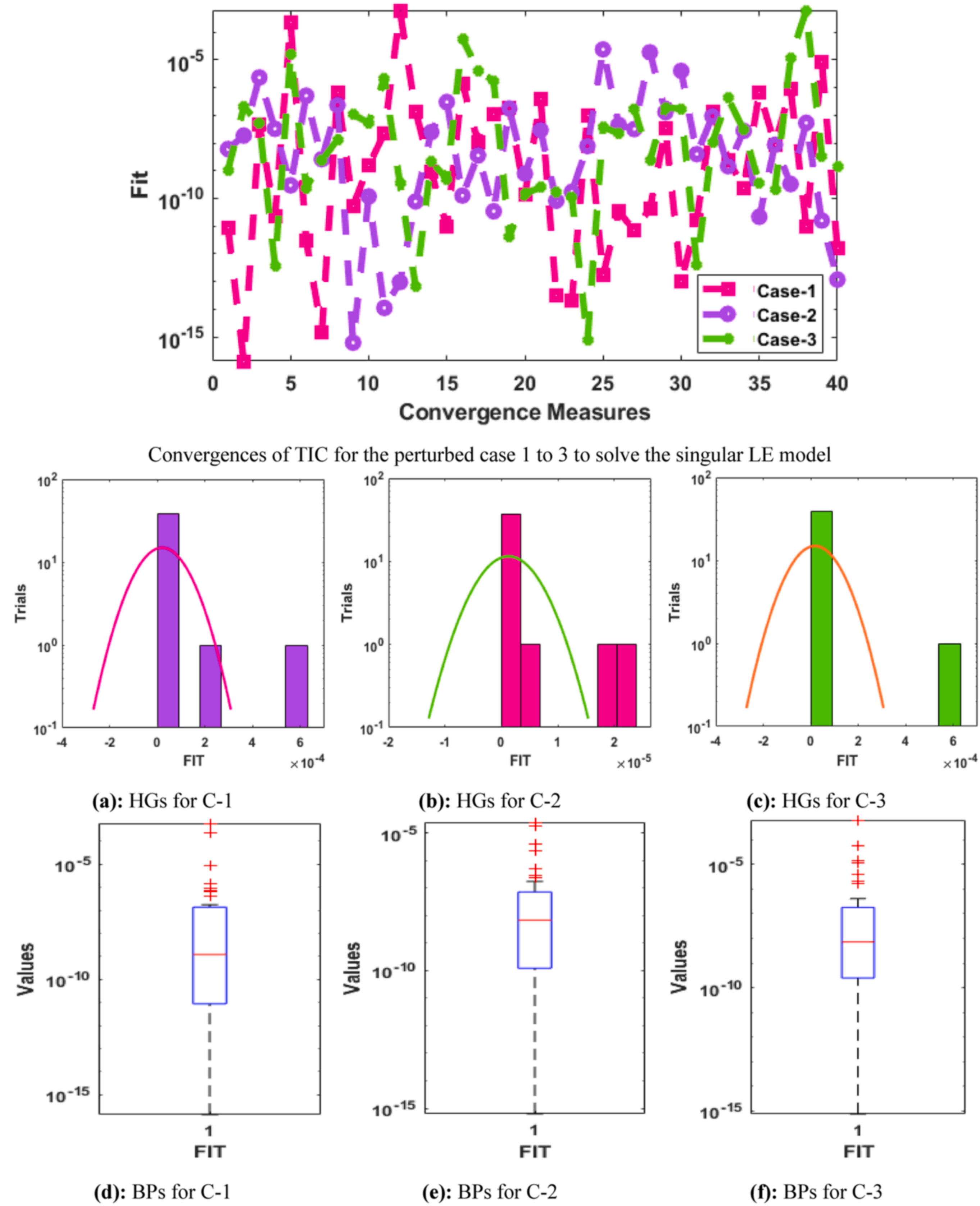

Fig. 5. Convergence of Fit for each perturbed case to solve the singular system.

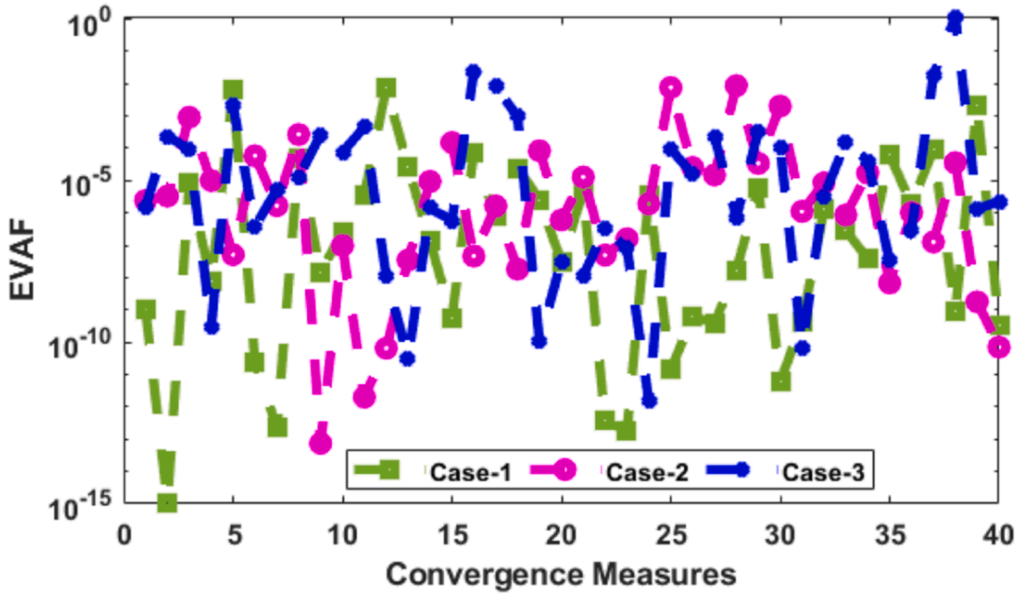

Convergences of EVAF for the perturbed case 1 to 3 to solve the singular EF system

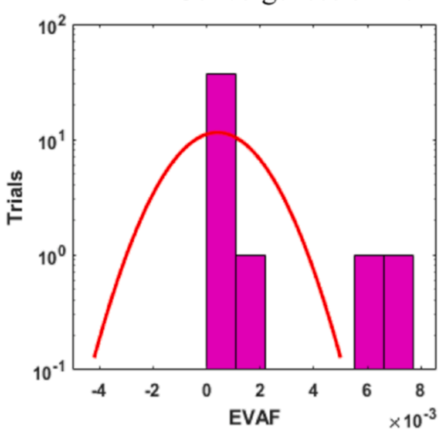

(a): HGs for C-1

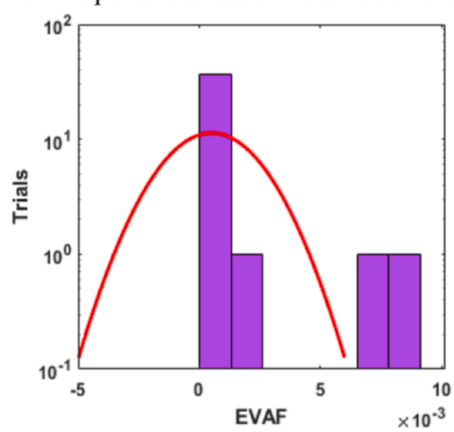

(b): HGs for C-2

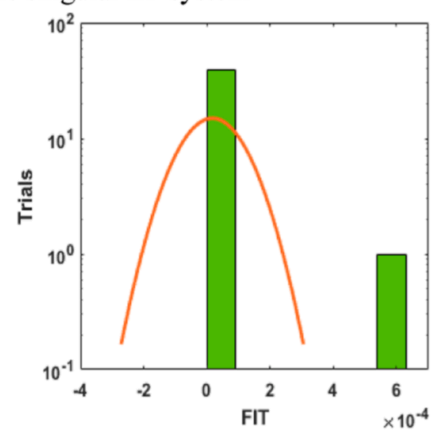

(c): HGs for C-3

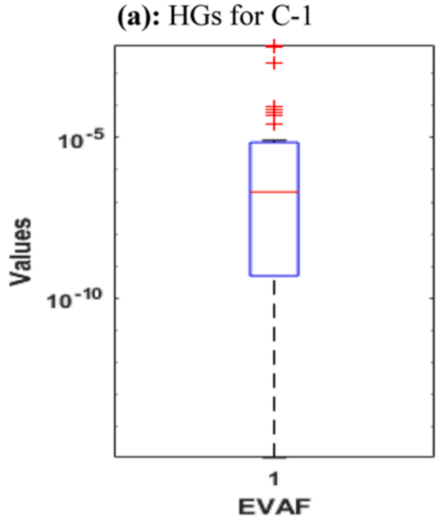

(d): BPs for C-1

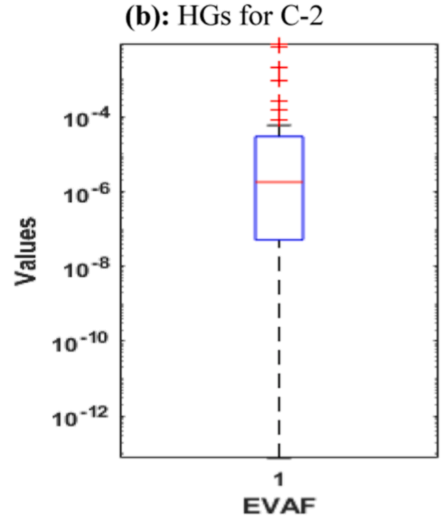

(e): BPs for C-2

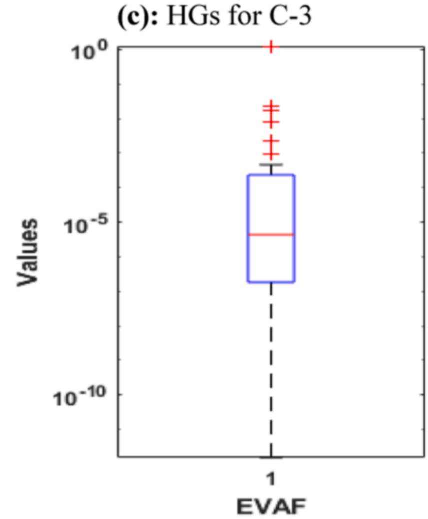

(f): BPs for C-3

Fig. 6. Convergence of EVAF for each perturbed case to solve the singular system.

Table 1
Statistics outcomes using the designed FMWNN-GAASA for perturbed case of the singular differential model.

Case	Operator	Statistical performances for the perturbed cases									
		0.1	0.2	0.3	0.4	0.5	0.6	0.7	0.8	0.9	1
1	Minimum	4×10^{-9}	7×10^{-9}	2×10^{-9}	4×10^{-9}	4×10^{-9}	6×10^{-9}	1×10^{-9}	1×10^{-9}	5×10^{-9}	2×10^{-9}
	Maximum	1×10^{-2}	2×10^{-2}	1×10^{-2}	8×10^{-3}	2×10^{-2}	2×10^{-2}	1×10^{-2}	3×10^{-3}	5×10^{-3}	8×10^{-3}
	Mean	8×10^{-4}	9×10^{-4}	8×10^{-4}	3×10^{-4}	8×10^{-4}	7×10^{-4}	5×10^{-4}	2×10^{-4}	3×10^{-4}	3×10^{-4}
	Median	8×10^{-5}	1×10^{-5}	3×10^{-5}	9×10^{-6}	1×10^{-5}	4×10^{-6}	5×10^{-6}	4×10^{-6}	6×10^{-6}	5×10^{-6}
	STD	2×10^{-3}	4×10^{-3}	3×10^{-3}	1×10^{-3}	3×10^{-3}	4×10^{-3}	2×10^{-3}	5×10^{-4}	9×10^{-4}	1×10^{-3}
	SIR	4×10^{-4}	7×10^{-5}	1×10^{-4}	6×10^{-5}	1×10^{-4}	3×10^{-5}	4×10^{-5}	2×10^{-5}	6×10^{-5}	2×10^{-5}
2	Minimum	4×10^{-8}	3×10^{-8}	2×10^{-8}	3×10^{-8}	7×10^{-9}	2×10^{-8}	7×10^{-9}	9×10^{-9}	2×10^{-8}	7×10^{-9}
	Maximum	3×10^{-2}	9×10^{-3}	7×10^{-3}	6×10^{-3}	5×10^{-3}	4×10^{-3}	3×10^{-3}	2×10^{-3}	3×10^{-3}	1×10^{-3}
	Mean	2×10^{-3}	6×10^{-4}	5×10^{-4}	4×10^{-4}	3×10^{-4}	2×10^{-4}	2×10^{-4}	2×10^{-4}	2×10^{-4}	1×10^{-4}
	Median	4×10^{-4}	3×10^{-5}	7×10^{-5}	4×10^{-5}	4×10^{-5}	2×10^{-5}	2×10^{-5}	2×10^{-5}	5×10^{-5}	2×10^{-5}
	STD	2×10^{-3}	4×10^{-3}	3×10^{-3}	1×10^{-4}	3×10^{-3}	4×10^{-3}	2×10^{-3}	5×10^{-3}	9×10^{-3}	1×10^{-3}
	SIR	7×10^{-4}	2×10^{-4}	1×10^{-4}	9×10^{-5}	9×10^{-5}	6×10^{-5}	5×10^{-5}	6×10^{-5}	6×10^{-5}	3×10^{-5}
3	Minimum	3×10^{-7}	7×10^{-8}	7×10^{-8}	3×10^{-8}	2×10^{-8}	3×10^{-8}	6×10^{-8}	1×10^{-8}	3×10^{-8}	5×10^{-8}
	Maximum	3×10^{-2}	9×10^{-3}	7×10^{-3}	6×10^{-3}	5×10^{-3}	4×10^{-3}	3×10^{-3}	2×10^{-3}	3×10^{-3}	1×10^{-3}
	Mean	1×10^{-2}	4×10^{-3}	2×10^{-3}	2×10^{-3}	1×10^{-3}	1×10^{-3}	8×10^{-4}	5×10^{-4}	5×10^{-4}	3×10^{-4}
	Median	6×10^{-3}	9×10^{-3}	1×10^{-4}	6×10^{-5}	7×10^{-5}	4×10^{-5}	6×10^{-5}	2×10^{-5}	6×10^{-5}	3×10^{-5}
	STD	2×10^{-3}	4×10^{-3}	3×10^{-3}	1×10^{-3}	3×10^{-3}	4×10^{-3}	2×10^{-3}	5×10^{-4}	9×10^{-4}	1×10^{-3}
	SIR	2×10^{-3}	3×10^{-4}	5×10^{-4}	2×10^{-4}	3×10^{-4}	1×10^{-4}	2×10^{-4}	6×10^{-5}	2×10^{-4}	6×10^{-5}

The proposed outcomes are provided in Eqs. (36)–(38) together with the graphical presentations are presented in Fig. 7(a–c), while the mean, best and worst results comparison is provided in Fig. 7(d–f) for the fractional case 1 to 3. The overlapping of the mean, best and worst results is performed for each FO case, which represent the exactness of the FMWNN-GAASA approach. The AE performances are presented in Fig. 7 (g) for the FO case of the singular differential model. The best AE performances are reported as 10^{-06} to 10^{-09}, 10^{-05} to 10^{-07} and 10^{-06} to 10^{-08} for 1st, 2nd and 3rd case. It is observed that the FO derivative is performed good for case 1 as compared to other two cases. Fig. 8 shows the performance measures for the FO case 1 to 3 to solve the singular differential model. The scale of the performance gages using the Fit, VAF and MSE operators for each perturbed case is given in Fig. 8. The Fit performances calculated closed to 10^{-15}, 10^{-13} for FO cases 1 and 2, while for the FO case 3, the Fit measures lie between 10^{-14} and 10^{-15}. The EVAF measures are calculated FO cases 1 to 3 closed to 10^{-11} and 10^{-12}, 10^{-09} and 10^{-10} and 10^{-11} and 10^{-12} to solve the singular differential model. The MSE measures for FO model are calculated for cases 1 and 2 closed to 10^{-11} and 10^{-12}, 10^{-09} and 10^{-10}, while for case 3 the performances are closed to 10^{-11} to solve the singular differential model. It is observed that these performances indicate that the case 1 performs very well as compared to other two FO derivative cases.

The convergence plots based on the statistical Fit, VAF and MSE together with HGs and BPs are derived in Figs. 9 and 10. The Fit measures are derived in Fig. 9 FO case of the singular model. The Fit values are calculated as 10^{-05} to 10^{-15}, 10^{-05} to 10^{-12}, 10^{-05} to 10^{-13} for each FO case of the singular model. The EVAF measures are reported in Fig. 10, which is around 10^{-05} to 10^{-12}, 10^{-03} to 10^{-10} and 10^{-05} to 10^{-11} for each FO case of the singular model. It is concluded on the behalf of these results that more than 80% executions achieved reasonable and precise level of the statistical results. The performances of these plots indicate that the case 1 performs is better as compared to other two FO derivative cases of the singular differential model.

The analysis of the FO factor is further analyzed in Table 2 by taking minimum, maximum, STD, mean, SIR and median operators for 40 executions to solve the singular models. The minimum values represent the good performances, while the opposite behavior is noticed in the case of maximum operators. The minimum values for the FO case are provided as 10^{-08} to 10^{-09}, 10^{-06} to 10^{-07} and 10^{-07} to 10^{-09}. The maximum gages are performed even bad result and found as 10^{-01} to 10^{-03} for each FO case of the singular model. The mean measures for the FO case are performed as 10^{-04} to 10^{-05}, 10^{-03} to 10^{-04} and 10^{-03} to 10^{-05}. The median representations for the FO case 1–3 are reported as 10^{-04} to 10^{-05}, 10^{-03} to 10^{-05} and 10^{-03} to 10^{-06}. The STD measures for the FO case of the model are reported as 10^{-02} to 10^{-03}. Similarly, the SIR performances are reported in good measures for each FO case 1–3 are reported as 10^{-04} to 10^{-06}, 10^{-03} to 10^{-05} and 10^{-03} to 10^{-06}.

The analysis of the FO performances of three cases is presented that the values of the $\beta = 0.1$ is performed betters as compared to the values of the $\beta = 0.2$ and $\beta = 0.3$. Few witnessed points that present the performance of case 1 is better as compared to case 2 and case 3 are presented as:

- The best AE performances are reported as 10^{-06} to 10^{-09}, 10^{-05} to 10^{-7} and 10^{-06} to 10^{-08} for case 1 to 3.
- The Fit operator performances are provided closed to 10^{-15}, 10^{-13} for FO cases 1 and 2, while for the FO case 3, the Fit measures lie between 10^{-14} and 10^{-15}.
- The EVAF measures for the FO cases 1 to 3 closed to 10^{-11} and 10^{-12}, 10^{-09} and 10^{-10}, 10^{-11} and 10^{-12} to solve the singular differential model.
- The MSE measures for FO cases 1 and 2 closed to 10^{-11} and 10^{-12}, 10^{-09} and 10^{-10}, while for case 3 the performances are closed to 10^{-11} for the singular differential model.

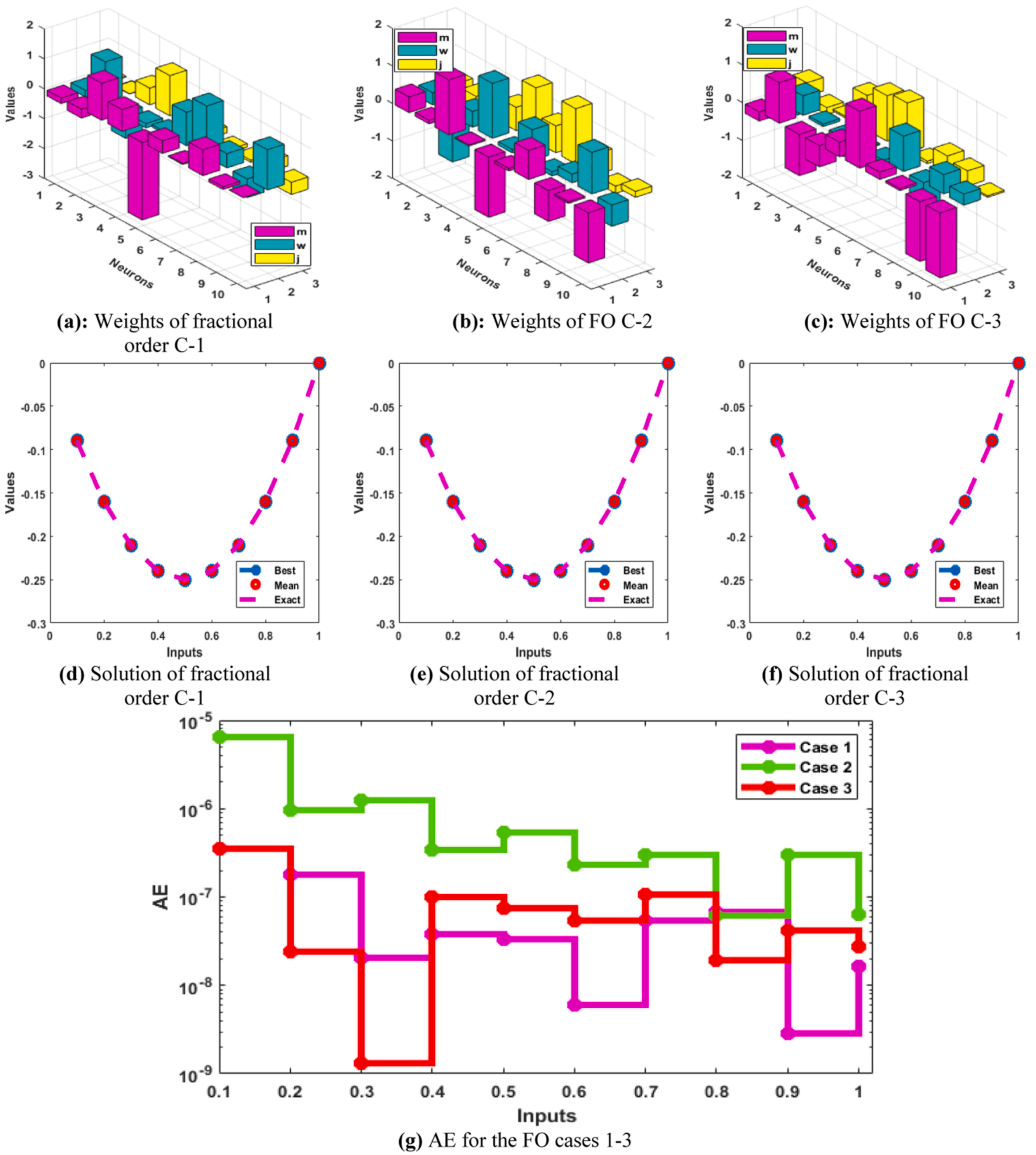

Fig. 7. Weights (a–c), solutions performances (d–f) and AE for the FO case 1 to 3 for solving the singular differential model.

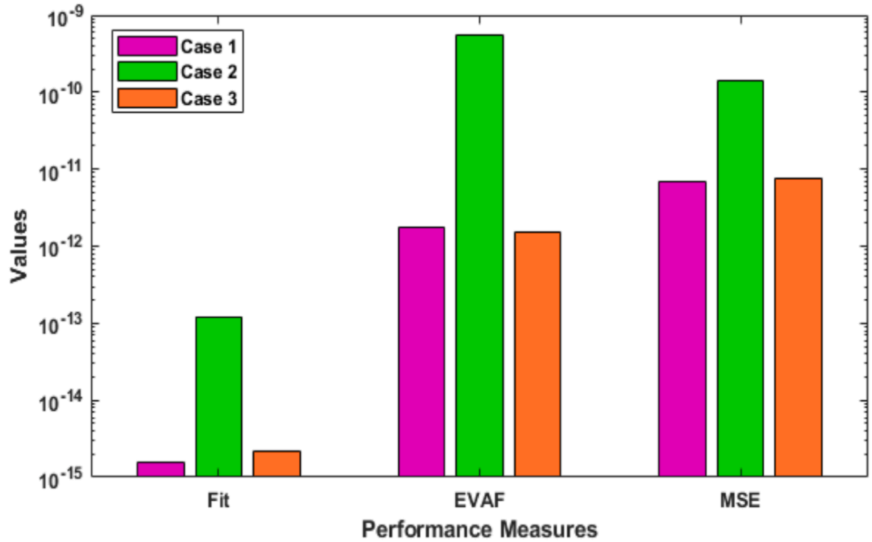

Fig. 8. Performance measures for the FO case 1 to 3 to solve the singular differential model.

- The convergence based on the Fitness is calculated as 10^{-05} to 10^{-15}, 10^{-05} to 10^{-12}, 10^{-05} to 10^{-13} for respective FO cases of the singular model.
- The EVAF are reported as 10^{-05} to 10^{-12}, 10^{-03} to 10^{-10} and 10^{-05} to $10^{-11}$for each FO case of the singular model.
- The minimum operator values for the respective FO cases are provided as 10^{-08} to 10^{-09}, 10^{-06} to 10^{-07} and 10^{-07} to 10^{-09}.
- The mean measures for the FO cases are performed as 10^{-04} to 10^{-05}, 10^{-03} to 10^{-04} and 10^{-03} to 10^{-05}.
- The median representations for the FO cases 1–3 are reported as 10^{-04} to 10^{-05}, 10^{-03} to 10^{-05} and 10^{-03} to 10^{-06}.

5. Conclusions

The current study presents an analysis of the perturbation factors and FO derivatives to solve the novel singular LE model. The singular models are very important, historical, and always challenging to solve due to the singularity at the origin. The perturbed FO design is presented first time by using the traditional LE model along with the detail of singular points, FO, shape, and perturbed factors. Few concluding remarks of this study are presented as:

- The design of perturbed fraction order singular model is presented by using the traditional form of the LE.
- The numerical investigations of the perturbation and FO terms has been performed by designing the novel FMWNN along with the global and local search effectiveness of the GAASA.
- The modeling based on the FMWNN is presented using the designed perturbed FO singular model in terms of mean square error sense, while the optimization is performed through the GAASA.
- The authentication, validation, excellence, and correctness of the perturbed FO singular model has been observed by using the comparative performances of the obtained and the reference solutions based on the perturbation and FO terms.
- The analysis of the perturbation factors and FO terms in the singular LE model has been provided in two different steps by taking three different values of the perturbed term as well as FO derivatives.
- The analysis of the perturbed singular and FO derivatives for three different cases has been presented and it is performed that the results of case 1 for both are more betters as compared to the other two cases.
- The analysis of both the perturbed singular and FO derivatives is performed through the plots of AE, performance indices, convergence analysis, EVAF, MSE and other statistical operators like minimum, mean, SIR, median and STD.

Future research directions

The analysis of the perturbation factors and FO derivatives to solve the novel singular LE model is presented in this study. In upcoming work, the analysis of the FO derivative values can be performed by taking the values close to 1. The analysis is performed in the future by taking the biological models, fluid models and other nonlinear differential models [84–90].

Impact statement

In this paper, we consider the well-known Lakshmanan-Porsezian-Daniel (LPD) Eq. (1) which describe the effect on the integrable properties of Heisenberg bilinear spin chains under the classical limit by the biquadratic interactions. The Lax pair have been driven via the AKNS scheme and the soliton solutions have been obtained via the inverse scattering transformation (IST) method. The obtained solutions based on different choices for the arbitrary constants α and β have been graphically represents.

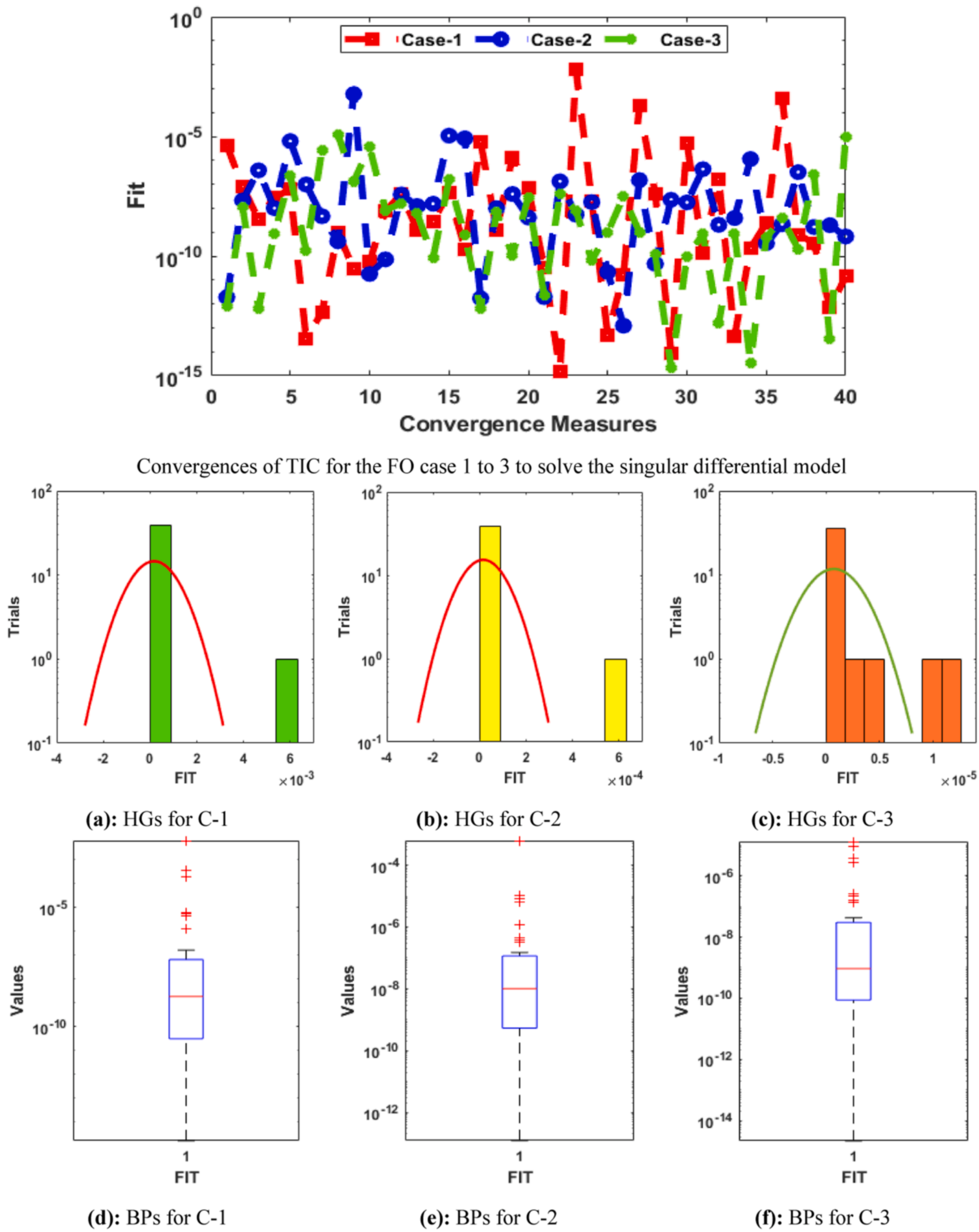

Fig. 9. Convergence of Fit for each FO case to solve the singular system.

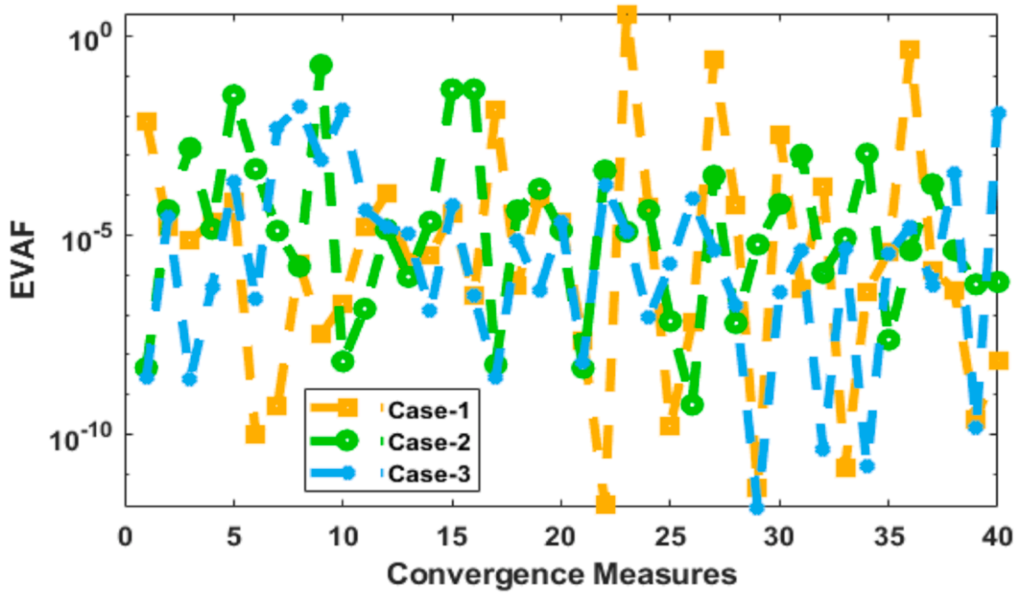

Convergences of EVAF for the FO case 1 to 3 to solve the singular differential model

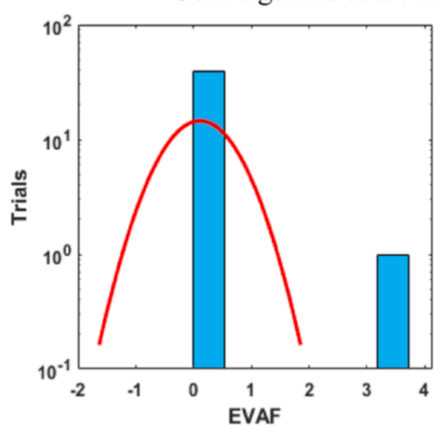

(a): HGs for C-1

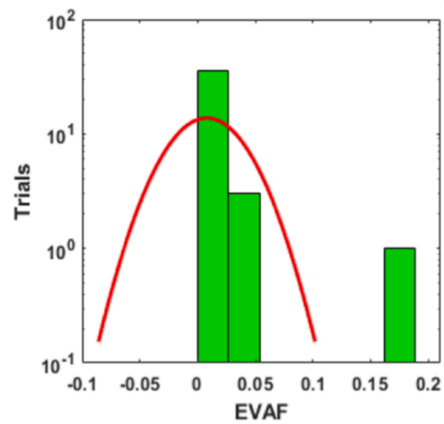

(b): HGs for C-2

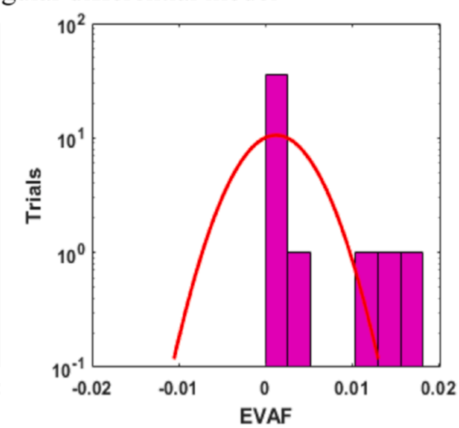

(c): HGs for C-3

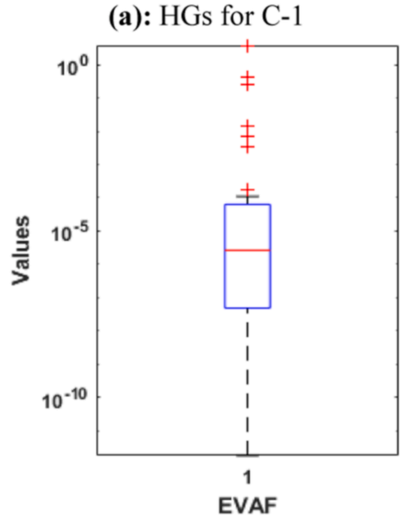

(d): BPs for C-1

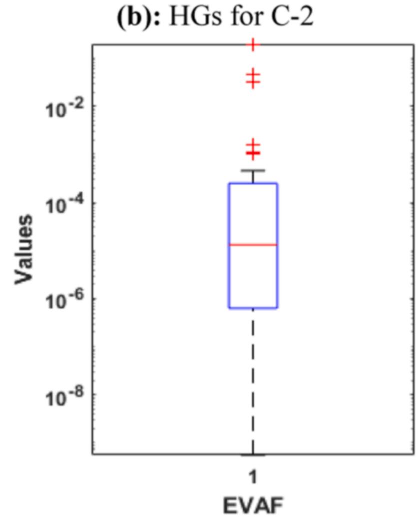

(e): BPs for C-2

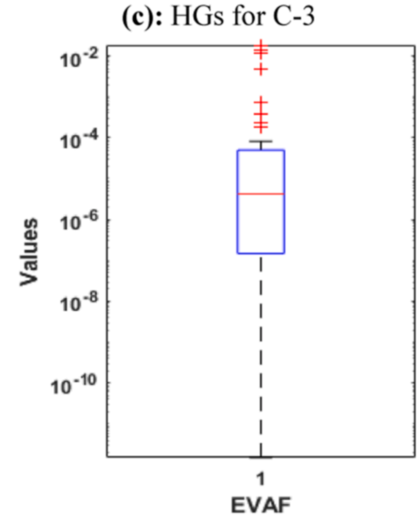

(f): BPs for C-3

Fig. 10. Convergence of EVAF for each FO case to solve the singular system.

Table 2
Statistics outcomes using the designed FMWNN-GAASA for each FO case of the singular differential model.

Case	Operator	Statistical measures for the FO cases									
		0.1	0.2	0.3	0.4	0.5	0.6	0.7	0.8	0.9	1
1	Minimum	7×10^{-8}	3×10^{-8}	2×10^{-8}	4×10^{-9}	3×10^{-8}	6×10^{-9}	5×10^{-8}	3×10^{-8}	3×10^{-9}	3×10^{-9}
	Maximum	2×10^{-1}	5×10^{-1}	3×10^{-1}	5×10^{-2}	7×10^{-2}	1×10^{-1}	2×10^{-1}	1×10^{-2}	1×10^{-1}	6×10^{-3}
	Mean	1×10^{-4}	2×10^{-5}	1×10^{-4}	3×10^{-4}	4×10^{-4}	4×10^{-4}	4×10^{-4}	1×10^{-5}	4×10^{-5}	3×10^{-5}
	Median	5×10^{-4}	7×10^{-5}	1×10^{-4}	5×10^{-6}	6×10^{-6}	2×10^{-5}	4×10^{-5}	2×10^{-5}	4×10^{-5}	1×10^{-5}
	STD	4×10^{-2}	8×10^{-2}	5×10^{-2}	9×10^{-3}	1×10^{-2}	2×10^{-2}	3×10^{-2}	3×10^{-3}	2×10^{-2}	1×10^{-3}
	SIR	1×10^{-4}	4×10^{-4}	4×10^{-4}	2×10^{-4}	2×10^{-6}	1×10^{-4}	1×10^{-4}	1×10^{-4}	1×10^{-4}	5×10^{-6}
2	Minimum	7×10^{-6}	1×10^{-7}	3×10^{-7}	3×10^{-7}	5×10^{-7}	3×10^{-8}	3×10^{-7}	6×10^{-8}	3×10^{-7}	6×10^{-8}
	Maximum	9×10^{-2}	1×10^{-1}	1×10^{-1}	6×10^{-2}	6×10^{-3}	5×10^{-2}	2×10^{-2}	3×10^{-2}	3×10^{-2}	8×10^{-3}
	Mean	8×10^{-3}	4×10^{-3}	4×10^{-3}	2×10^{-3}	7×10^{-4}	1×10^{-3}	9×10^{-4}	9×10^{-4}	1×10^{-3}	3×10^{-4}
	Median	1×10^{-3}	2×10^{-4}	2×10^{-4}	9×10^{-5}	1×10^{-4}	7×10^{-5}	1×10^{-4}	4×10^{-5}	8×10^{-5}	3×10^{-5}
	STD	4×10^{-2}	8×10^{-2}	5×10^{-2}	9×10^{-3}	1×10^{-2}	2×10^{-2}	3×10^{-2}	3×10^{-3}	2×10^{-2}	1×10^{-3}
	SIR	2×10^{-3}	5×10^{-4}	4×10^{-4}	2×10^{-4}	2×10^{-4}	9×10^{-5}	1×10^{-4}	7×10^{-5}	1×10^{-4}	3×10^{-5}
3	Minimum	4×10^{-7}	2×10^{-8}	1×10^{-9}	1×10^{-7}	3×10^{-9}	5×10^{-8}	2×10^{-8}	2×10^{-8}	8×10^{-9}	6×10^{-9}
	Maximum	9×10^{-2}	1×10^{-1}	1×10^{-1}	6×10^{-2}	6×10^{-3}	5×10^{-2}	2×10^{-2}	3×10^{-2}	3×10^{-2}	8×10^{-3}
	Mean	4×10^{-3}	1×10^{-3}	8×10^{-4}	5×10^{-4}	6×10^{-4}	4×10^{-4}	3×10^{-4}	4×10^{-4}	3×10^{-4}	9×10^{-5}
	Median	6×10^{-3}	1×10^{-3}	8×10^{-5}	3×10^{-5}	3×10^{-5}	2×10^{-5}	4×10^{-5}	1×10^{-5}	4×10^{-5}	6×10^{-6}
	STD	4×10^{-2}	8×10^{-2}	5×10^{-2}	9×10^{-3}	1×10^{-2}	2×10^{-2}	3×10^{-2}	3×10^{-3}	2×10^{-2}	1×10^{-3}
	SIR	8×10^{-4}	2×10^{-4}	1×10^{-4}	1×10^{-4}	1×10^{-4}	8×10^{-5}	8×10^{-5}	4×10^{-5}	9×10^{-5}	1×10^{-5}

Data availability statement

Not applicable.

Declaration of Competing Interest

The authors declare that they have no known competing financial interests or personal relationships that could have appeared to influence the work reported in this paper.

Data availability

Data will be made available on request.

References

[1] Wazwaz AM. Adomian decomposition method for a reliable treatment of the Emden–Fowler equation. Appl Math Comput 2005;161(2):543–60.
[2] Sabir Z, et al. Integrated intelligence of neuro-evolution with sequential quadratic programming for second-order Lane–Emden pantograph models. Math Comput Simul 2021;188:87–101.
[3] Wong JS. On the generalized Emden–Fowler equation. SIAM Rev 1975;17(2):339–60.
[4] Sabir Z, et al. Neuro-evolution computing for nonlinear multi-singular system of third order Emden–Fowler equation. Math Comput Simul 2021;185:799–812.
[5] Sabir Z, Raja MAZ, Baleanu D. Fractional mayer neuro-swarm heuristic solver for multi-fractional order doubly singular model based on lane–emden equation. Fractals 2021;29(05):2140017.
[6] Sabir Z, Khalique CM, Raja MAZ, Baleanu D. Evolutionary computing for nonlinear singular boundary value problems using neural network, genetic algorithm and active-set algorithm. Eur Phys J Plus 2021;136(2):1–19.
[7] Sabir Z, et al. Numerical investigations to design a novel model based on the fifth order system of Emden–Fowler equations. Theor Appl Mech Lett 2020;10(5):333–42.
[8] Abdelkawy MA, et al. Numerical investigations of a new singular second-order nonlinear coupled functional Lane–Emden model. Open Phys 2020;18(1):770–8.
[9] Adel W, et al. Solving a new design of nonlinear second-order Lane–Emden pantograph delay differential model via Bernoulli collocation method. Eur Phys J Plus 2020;135(5):1–12.
[10] Wazwaz AM. A new algorithm for solving differential equations of Lane–Emden type. Appl Math Comput 2001;118(2–3):287–310.
[11] Liao S. A new analytic algorithm of Lane–Emden type equations. Appl Math Comput 2003;142(1):1–16.
[12] Sabir Z, et al. On a new model based on third-order nonlinear multisingular functional differential equations. Math Probl Eng 2020;2020:1–12.
[13] Yousefi SA. Legendre wavelets method for solving differential equations of Lane–Emden type. Appl Math Comput 2006;181(2):1417–22.
[14] Roul P, et al. An optimal sixth-order quartic B-spline collocation method for solving Bratu-type and Lane-Emden–type problems. Math Methods Appl Sci 2019;42(8):2613–30.
[15] Mall S, et al. Chebyshev neural network based model for solving Lane–Emden type equations. Appl Math Comput 2014;247:100–14.
[16] Bhrawy AH, Alofi AS. A Jacobi–Gauss collocation method for solving nonlinear Lane–Emden type equations. Commun Nonlinear Sci Numer Simul 2012;17(1):62–70.
[17] Parand K, et al. A numerical approach to solve Lane-Emden type equations by the fractional order of rational Bernoulli functions. Rom J Phys 2017;62(104):1–24.
[18] Parand K, et al. Two efficient computational algorithms to solve the nonlinear singular Lane-Emden equations. Astrophysics 2020;63(1):133–50.
[19] Delkhosh M, et al. Accurate numerical solution for a type of astrophysics equations using three classes of Euler functions. Bulletin mathématique de la Société des. Sci Math Roum 2018;61(1):39–49.
[20] Izadi M. A discontinuous finite element approximation to singular Lane-Emden type equations. Appl Math Comput 2021;401:126115.
[21] Singh H, et al. A reliable algorithm for the approximate solution of the nonlinear Lane-Emden type equations arising in astrophysics. Numer Methods Partial Differ Equ 2018;34(5):1524–55.
[22] Mosavi A, et al. Machine learning for modeling the singular multi-pantograph equations. Entropy 2020;22(9):1041.
[23] Sabir Z, et al. A novel design of fractional Meyer wavelet neural networks with application to the nonlinear singular fractional Lane-Emden systems. Alex Eng J 2021;60(2):2641–59.
[24] Sabir Z, Baleanu D, Raja, et al. Design of neuro-swarming heuristic solver for multi-pantograph singular delay differential equation. Fractals 2021;29(05):2140022.
[25] Sabir Z, et al. Integrated intelligent computing with neuro-swarming solver for multi-singular fourth-order nonlinear Emden–Fowler equation. Comput Appl Math 2020;39(4):1–18.
[26] Sabir Z, Baleanu D, et al. Design of stochastic numerical solver for the solution of singular three-point second-order boundary value problems. Neural Comput Appl 2021;33(7):2427–43.
[27] Sabir Z, et al. Integrated intelligent computing paradigm for nonlinear multi-singular third-order Emden–Fowler equation. Neural Comput Appl 2021;33(8):3417–36.
[28] Chandrasekhar S. An introduction to the study of stellar structure. New York: Dover Publications; 1967.
[29] Yu F. Integrable coupling system of fractional soliton equation hierarchy. Phys Lett A 2009;373(41):3730–3.
[30] Momani S, et al. On a fractional integral equation of periodic functions involving Weyl–Riesz operator in Banach algebras. J Math Anal Appl 2008;339(2):1210–9.
[31] Diethelm K, et al. Analysis of fractional differential equations. J Math Anal Appl 2002;265(2):229–48.
[32] Ibrahim RW, et al. On the existence and uniqueness of solutions of a class of fractional differential equations. J Math Anal Appl 2007;334(1):1–10.
[33] Bonilla B, et al. On systems of linear fractional differential equations with constant coefficients. Appl Math Comput 2007;187(1):68–78.
[34] Shah K, et al. Semi-analytical study of Pine Wilt Disease model with convex rate under Caputo–Febrizio fractional order derivative. Chaos Solitons Fractals 2020;135:109754.
[35] Yang XJ, et al. A new general fractional-order derivataive with Rabotnov fractional-exponential kernel applied to model the anomalous heat transfer. Therm Sci 2019;23(3 Part A):1677–81.
[36] Elsonbaty AMR, et al. Dynamical analysis of a novel discrete fractional SITRs model for COVID-19. Fractals 2021;46:2140035.
[37] Owolabi KM, et al. Spatiotemporal patterns in the Belousov–Zhabotinskii reaction systems with Atangana–Baleanu fractional order derivative. Physica A 2019;523:1072–90.
[38] Ghanbari B, et al. Mathematical and numerical analysis of a three-species predator-prey model with herd behavior and time fractional-order derivative. Math Methods Appl Sci 2020;43(4):1736–52.

[39] Hong Y, et al. Application of fractional-order derivative in the quantitative estimation of soil organic matter content through visible and near-infrared spectroscopy. Geoderma 2019;337:758–69.
[40] Akkilic, A.N., et al., 2022 Numerical treatment on the new fractional-order SIDARTHE COVID-19 pandemic differential model via neural networks. Eur Phys J Plus, 137(3), pp.1–14.
[41] Din A, et al. On analysis of fractional order mathematical model of Hepatitis B using Atangana–Baleanu Caputo (ABC) derivative. Fractals 2022;30(01):2240017.
[42] Sabir Z, Umar M, Raja MAZ, Baleanu D. Applications of Gudermannian neural network for solving the SITR fractal system. Fractals 2021;78:1.
[43] Guirao JL, et al. Design of neuro-swarming computational solver for the fractional Bagley–Torvik mathematical model. Eur Phys J Plus 2022;137(2):245.
[44] Junsawang P, et al. Numerical simulations of vaccination and wolbachia on dengue transmission dynamics in the nonlinear model. IEEE Access 2022;10:31116–44.
[45] Farrell PA, et al. Robust computational techniques for boundary layers. New York: Chapman-Hall/CRC; 2000.
[46] Doolan EP, et al. Uniform numerical methods for problems with initial and boundary layers. Boole Press; 1980.
[47] Roos HG, et al. Numerical methods for singularly perturbed differential equations, convection diffusion and flow problems. Berlin: Springer Verlag; 1996.
[48] Linss T, et al. A hybrid difference scheme on a Shishkin mesh for linear convection-diffusion problems. Appl Numer Math 1999;31:255–70.
[49] Erdogan F, et al. A finite difference method on layer-adapted mesh for singularly perturbed delay differential equations. Appl Math Nonlinear Sci 2020;5(1):425–36.
[50] Miller JJH, et al. Fitted numerical methods for singular perturbation problems. error estimates in the maximum norm for linear problems in one and two dimensions. Singapore: World Scientific; 1996.
[51] Linss T. Layer-adapted meshes for convection Â–diffusion problems. Comput Methods Appl Mech Eng 2003;192(9Â–10):1061–105.
[52] Phaneendra K, et al. A fitted numerov method for singular perturbation problems exhibiting twin layers. Appl Math Inf Sci 2010;4(3):341–52.
[53] Patidar KC. High order fitted operator numerical method for self-adjoint singular perturbation problems. Appl Math Comput 2005;171:547–66.
[54] Holevoet D, et al. The optimal exponentially-fitted numerov method for solving two-point boundary value problems. J Comput Appl Math 2010;230:260–9.
[55] Amiraliyeva IG. A uniform numerical method for dealing with a singularly perturbed delay inital value problem. Appl Math Lett 2010;23:1221–5.
[56] Kopteva N, et al. Numerical analysis of a singularly perturbed nonlinear reaction–diffusion problem with multiple solutions. Appl Numer Math 2004;51 (2–3):273–88.
[57] Bawa RK. A Paralel aproach for self-adjoint singular perturbation problems using Numerov's scheme, nternational. J Comput Math 2007;84(3):317–23.
[58] Patidar KC. High order fitted operator numerical method for self-adjoint singular perturbation problems. Appl Math Comput 2005;171:547–66.
[59] Shahid N, et al. Applications of artificial neural networks in health care organizational decision-making: a scoping review. PLoS ONE 2019;14(2): e0212356.
[60] Niazkar HR, et al. Application of artificial neural networks to predict the COVID-19 outbreak. Glob Health Res Policy 2020;5(1):1–11.
[61] Sabir Z, Raja MAZ, Baleanu D, et al. Investigations of nonlinear induction motor model using the Gudermannian neural networks. Therm Sci 2021;99(00):261.
[62] Horak J, et al. Support vector machine methods and artificial neural networks used for the development of bankruptcy prediction models and their comparison. J Risk Financ Manag 2020;13(3):60.
[63] Rostami S, et al. Forecasting the thermal conductivity of a nanofluid using artificial neural networks. J Therm Anal Calorim 2021;145(4):2095–104.
[64] Sabir Z. Neuron analysis through the swarming procedures for the singular two-point boundary value problems arising in the theory of thermal explosion. Eur Phys J Plus 2022;137(5):1–18.
[65] Sabir Z, et al. Neuron analysis of the two-point singular boundary value problems arising in the thermal explosion's theory. Neural Processing Letters; 2022. p. 1–28.
[66] Bre F, et al. Prediction of wind pressure coefficients on building surfaces using artificial neural networks. Energy Build 2018;158:1429–41.
[67] Afzaal H, et al. Groundwater estimation from major physical hydrology components using artificial neural networks and deep learning. Water 2019;12(1): 5 (Basel).
[68] Imtiaz SI, et al. DeepAMD: detection and identification of android malware using high-efficient deep artificial neural network. Future Gener Comput Syst 2021;115: 844–56.
[69] Getahun MA, et al. Artificial neural network based modelling approach for strength prediction of concrete incorporating agricultural and construction wastes. Constr Build Mater 2018;190:517–25.
[70] Sabir Z, et al. Dynamics of multi-point singular fifth-order Lane–Emden system with neuro-evolution heuristics. Evolv Syst 2022;155:1–12.
[71] Sabir Z, et al. A neuro-evolution heuristic using active-set techniques to solve a novel nonlinear singular prediction differential model. Fractal Fract 2022;6(1):29.
[72] Adánez JM, et al. Multidimensional membership functions in T–S fuzzy models for modelling and identification of nonlinear multivariable systems using genetic algorithms. Appl Soft Comput 2019;75:607–15.
[73] Artar M, et al. Optimum weight design of steel space frames with semi-rigid connections using harmony search and genetic algorithms. Neural Comput Appl 2018;29(11):1089–100.
[74] Flórez CAC, et al. Control structure for a car-like robot using artificial neural networks and genetic algorithms. Neural Comput Appl 2018;34:1–14.
[75] Zameer A, et al. Bio-inspired heuristics for layer thickness optimization in multilayer piezoelectric transducer for broadband structures. Soft Comput 2019;23 (10):3449–63.
[76] Akbar S, et al. Design of bio-inspired heuristic techniques hybridized with sequential quadratic programming for joint parameters estimation of electromagnetic plane waves. Wirel Pers Commun 2017;96(1):1475–94.
[77] Jamal R, et al. Hybrid bio-inspired computational heuristic paradigm for integrated load dispatch problems involving stochastic wind. Energies 2019;12(13):2568.
[78] Kim H, et al. Nonnegative matrix factorization based on alternating nonnegativity constrained least squares and active set method. SIAM J Matrix Anal Appl 2008;30 (2):713–30.
[79] Piller O, et al. A content-based active-set method for pressure-dependent models of water distribution systems with flow controls. J Water Resour Plann Manage 2020; 146(4):04020009.
[80] Zhang C, et al. A smoothing active set method for linearly constrained non-lipschitz nonconvex optimization. SIAM J Optim 2020;30(1):1–30.
[81] Noii N, et al. A quasi-monolithic phase-field description for orthotropic anisotropic fracture with adaptive mesh refinement and primal–dual active set method. Eng Fract Mech 2021;258:108060.
[82] Klaučo M, et al. Machine learning-based warm starting of active set methods in embedded model predictive control. Eng Appl Artif Intell 2019;77:1–8.
[83] Li Y, et al. An active-set algorithm for solving large-scale nonsmooth optimization models with box constraints. PLoS ONE 2018;13(1):e0189290.
[84] Sabir Z, et al. Design of Morlet wavelet neural network to solve the non-linear influenza disease system. Appl Math Nonlinear Sci 2022:271–86.
[85] Baleanu D, et al. On some new properties of fractional derivatives with Mittag-Leffler kernel. Commun Nonlinear Sci Numer Simul 2018;59:444–62.
[86] Yokuş A, et al. Numerical solutions with linearization techniques of the fractional Harry Dym equation. Appl Math Nonlinear Sci 2019;4(1):35–42.
[87] Dewasurendra M, et al. On the method of inverse mapping for solutions of coupled systems of nonlinear differential equations arising in nanofluid flow, heat and mass transfer. Appl Math Nonlinear Sci 2018;3(1):1–14.
[88] Baleanu D, et al. Analysis of the model of HIV-1 infection of CD4+ $ CD4ˆ{+} $ T-cell with a new approach of fractional derivative. Adv Differ Equ 2020;2020(1): 1–17.
[89] Qin Y, et al. Research on relationship between tourism income and economic growth based on meta-analysis. Appl Math Nonlinear Sci 2018;3(1):105–14.
[90] Baleanu D, et al. Fractional calculus: models and numerical methods. World Scientific; 2012 (Vol. 3).